SAR Advanced Deployable Structure

S. Pellegrino, C. Green, S.D. Guest
and A. Watt

CUED/D-STRUCT/TR191

The work presented in this report was partially supported by research contract no. 19673/0040300096/SUB between Matra Marconi Space UK Limited and the University of Cambridge. Technical monitor: Martin Cohen.

Release date: 18 November, 2000.

Summary

This report presents a series of preliminary studies into novel concepts for the next generation of SAR structures. The report is divided into two self-contained parts.

Part 1 begins with a study of the behaviour of tape-spring hinges; this is a type of self-deploying and self-locking hinge that offers some considerable advantages over conventional hinges for deployable structures. After deriving design formulas for these hinges, a novel implementation of tape-spring hinges is developed. The results of preliminary tests on demonstration hardware are presented.

Part 2 is a study of a novel approach to deployable SAR structures that builds upon recent work on inflatable SAR structures at NASA JPL. This approach is based on TR modules that are attached to a flexible structure, such as a Kapton membrane. This membrane is deployed and held in a pre-stressed, flat configuration by an edge frame that is, in turn, deployed by tape-spring hinges. Several concepts for frames that can be packaged very compactly as a bundle of bars have been identified and demonstration hardware for the most promising concepts has been made.

A system-level study of a deployable light SAR for a spacecraft to be launched on the ROCKOT vehicle is presented.

Contents

Chapter 1

Design of Tape-Spring Hinges

1.1 Introduction

The use of carpenter tapes, or tape springs (i.e. the curved metal tape found in tape measures) in designing self deploying hinges has been long considered (Luhman, Etzler and Wagner 1989, Seffen and Pellegrino 1997, Szyszkowski, Fielden and Johnson, 1997). In order to fold these tapes a large moment is required to initially buckle the tape, after buckling a much lower moment is required to continue folding the tape. During deployment the tapes provide a small but constant restoring moment and "lock" into the straight position.

Carpenter tapes can be used in the design of self-deploying, self-locking hinges without any moving parts, and they are increasingly being used as a replacement of more traditional hinge mechanisms for deployable structures applications. The references listed above show several different ways of arranging the blades, which are illustrated in Figure 1.1.

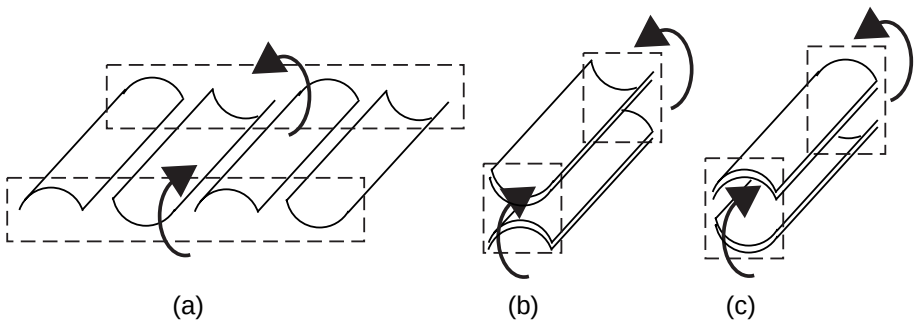

Figure 1.1: Different arrangements of four tape springs in a self-locking hinge.

Hinges based on any of these configurations will have the basic characteristics described above and in certain respects they perform in the same way. For example the deployment torque applied by these hinges will be approximately equal to the sum of the moments of its restoring tapes. However, the hinge in Figure 1.1(c) is superior for the following reasons.

- By connecting two tape springs in parallel with a small separation between

them the moment required to "unlock" the hinge increases as the tapes act predominantly in tension and compression, instead of bending as in Figure 1.1(a).

- The stiffness of the "locked" hinge is much higher, and can also be varied by varying the separation of the tapes, as well as the blade dimensions. Unlike the arrangement in Figure 1.1(b) the edges of the top tape springs are not subject to high compression, and hence are less prone to buckle locally.

- A kick-off restoring moment can be obtained at the beginning of deployment, due to the interaction between the two tapes.

A potential problem with deployable structures that make use of tape spring hinges is that these hinges are very "floppy" when they are folded, with translation and rotation occurring in unwanted directions. To ensure that the structure deploys as intended additional kinematic constraints have to be added, but over-complex designs should be avoided.

The addition of these constraints by the combination of a Rolamite hinge to the tape-spring hinge will be investigated. An approach of this kind was first proposed in the ADELE concept (Blanc 1990). An analysis of some of the design parameters for hinges of this type is presented, together with a new, more compact, simpler, and more efficient implementation of the concept.

1.2 Moment-Rotation Relationship

Detailed studies of a single tape-spring have been carried out by Seffen and Pellegrino (1999). Some of their results can be extrapolated to hinge consisting of two or more tape springs; indeed, for the hinge shown in Figure 1.1(a) the complete moment-rotation relationship can be obtained by superposing the relationships for each tape spring. However, for the hinge shown in Figure 1.1(c) there are some major differences as well.

The moment-rotation relationship for a hinge consisting of tape springs, as shown in Figure 1.1, has the general shape of Fig. 1.2.

Important points to note are as follows.

- The $M-\theta$ curve is symmetric about the origin, because the behaviour of the hinge does not change when the sign of the moment is reversed; this is because the arrangement of the tape springs is symmetric with respect to the centre plane.

- For small θ's the relationship is approximately linear, provided that $|M| < M_{max}$. The value of M_{max} is in the range 5-15 Nm for the hinges that have been made so far.

- As the rotation angle is further increased one of the tape springs snaps while M suddenly decreases, and an elastic "fold" starts forming in the middle of the hinge.

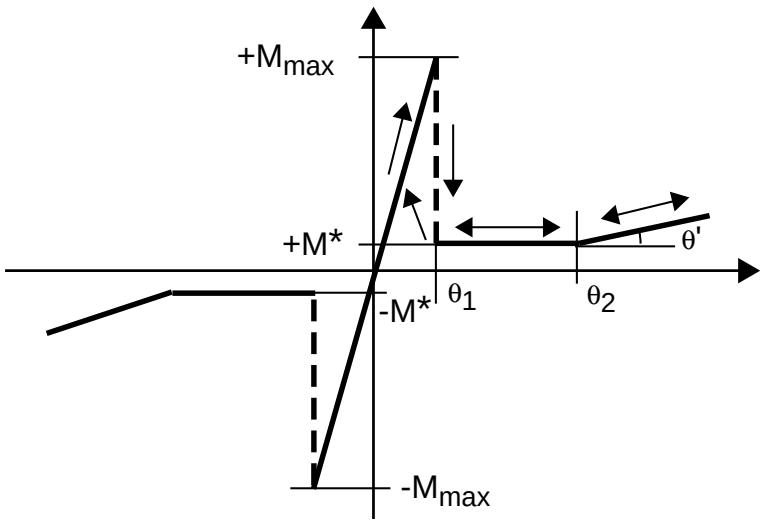

Figure 1.2: Typical moment-rotation relationship of tape-spring hinge.

- As θ is further increased, M remains approximately constant, $M \approx M^*$. At a value between one and two orders of magnitude less than M_{max}.
- For even larger θ's M slowly increases, as the folds in different tape springs interact with each other and/or the folds reach the end of the springs.

The values of M_{max} and M^* can be readily estimated, see the next section, but there are no general expressions for the other values, θ_1, θ_2, θ' that define the M-θ relationship.

1.3 Design Equations

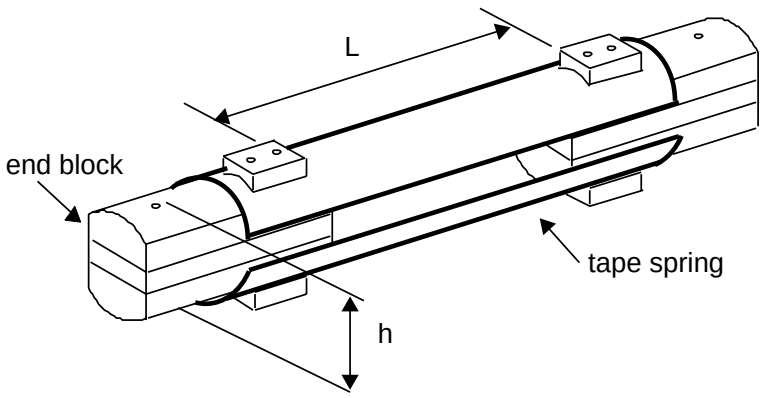

Figure 1.3: Tape-spring hinge.

Figure 1.3 shows a hinge consisting of two tape springs. The main geometric parameters are the (even) number n of tape springs, here $n = 2$, the length L

measured between the ends of the attachment blocks, and the separation h of the tape springs, see Figure 1.4. In addition, of course, the cross-sectional and material properties of the tape springs.

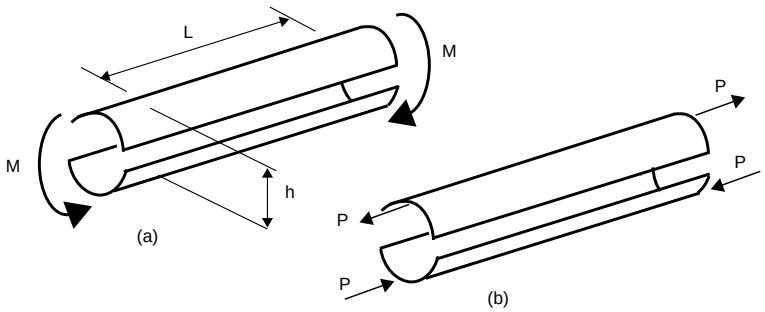

Figure 1.4: Loading of tape-springs in "straight" hinge configuration.

M_{max} can be estimated by multiplying the buckling load P_{cr} of the compression tape spring by the separation h, hence

$$M_{max} = P_{cr}h \tag{1.1}$$

where P_{cr} is obtained by solving Equation 1.12.

M^* is obtained by adding the steady-state moments required to form elastic folds in all the tape springs. Half of the springs are bent in the "opposite" sense and the other half in the "equal" sense and hence the corresponding moments are respectively, see Seffen and Pellegrino (1999),

$$2(1+\nu)D\alpha \quad \text{and} \quad 2(1-\nu)D\alpha$$

where

$$D = Et^3/12(1-\nu^2)$$

Here E, ν have the usual meaning, t is the thickness of the tape spring, and 2α is the angle subtended by its cross section.

Considering all tape springs

$$M^* = 2nD\alpha \tag{1.2}$$

1.4 Maximum Moment

The maximum moment, M_{max}, that can be carried by a hinge without snapping has been investigated. A simple analytical model that considers the critical stress of the compression tape spring —assumed to be straight up to the point of buckling— is not accurate. Hence, a more refined analysis is presented, which includes the effect of the eccentricity of P with respect to the axis of the tape spring, and hence its associated out-of-straightness on the point of buckling.

1.4.1 Buckling of straight tape spring

This analysis considered the compressed member in the hinge buckling either in an overall mode as a classical Euler strut, or in a local mode as a shell panel in compression.

The Euler buckling load is given by[1]

$$P_{crit} = \frac{\pi^2 EI}{L^2} \tag{1.3}$$

where I for a circular-arc section subtending an angle 2α is:

$$I = \alpha t r^3 \left(1 - 2\left(\frac{sin(\alpha)}{\alpha}\right)^2 + \frac{sin(2\alpha)}{(2\alpha)}\right) \tag{1.4}$$

The critical buckling stress of a shell in compression is (Allen and Bulson 1980):

$$\sigma_{crit} = \frac{Et}{r\sqrt{3(1-\nu^2)}} \tag{1.5}$$

with

$$P_{crit} = 2\alpha r t \sigma_{crit} \tag{1.6}$$

The lower value of these two critical buckling forces was chosen and then transformed into the critical buckling moment by multiplying by the separation distance. It was found that for practical lengths of these hinges Euler buckling was the dominant mode, local buckling giving very high results. Hence

$$M_{max} = \pi^2 EIh/L^2 \tag{1.7}$$

These predicted values of M_{max} were then compared to values obtained from non-linear finite element simulations and experiments by Laloi (1999). The results can be seen in Figure 1.5.

These predictions are far higher than the measured buckling moments, especially for short lengths. Because Eq. 1.7 is very sensitive to the value of L, the predictions could be made to appear much more accurate if one adjusted the value of L. A more sensible approach, though, is to refine the analysis.

1.4.2 Buckling of an eccentrically loaded tape-spring

This second analysis is based upon the following observations, made using the bending apparatus manufactured by Laloi (1999). The tape springs fitted in the apparatus were the longest that she had tested, $\approx$ 150 mm total length.

[1] Here it is being assumed that the wavelength of the buckling mode is equal to the length L defined in Figure 1.3, but this can be easily modified.

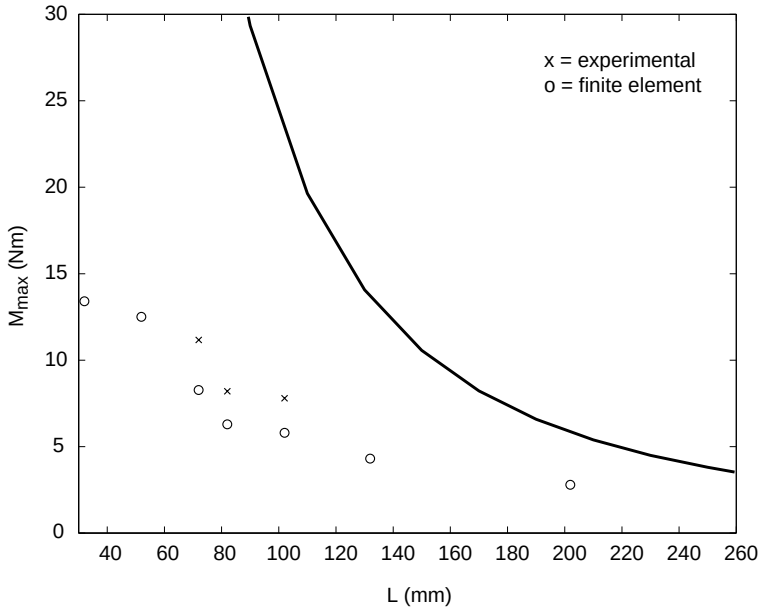

Figure 1.5: Comparison of Eq. 1.7 with experimental and finite-element results.

1. When two end moments are applied to the hinge, the tension spring immediately formes edge buckles, which grow in amplitude with increasing moment.

   The edges of the tension spring remain essentially unstressed: all the tension load is carried by a central strip of width approximately equal to the width of the end fittings.

2. The tension spring is essentially straight.

   The compression spring bends very significantly; its shape is very smooth and the edges seem perfectly stable, suggesting that they are in tension, although the spring is overall in compression.

   Shortly before buckling a central bowing amplitude of 2-3 mm is measured in the compression tape spring.

3. The buckling of the compression spring is very sudden and is accompanied by a large reduction of the load carried by the spring.

4. An analysis of the buckling of the compression spring as an Euler strut is inaccurate for the range of spring lengths that are practical but becomes quite accurate over 200 mm.

   An analysis based on a cylindrical panel that is simply supported on all edges vastly overestimates the buckling load. Also, it predicts a constant buckling load for tape springs of different lengths; this disagrees with both finite element and experimental analyses, which show a clear reduction in buckling load when the length increases.

The buckling of an edge panel, free on one edge, significantly underestimates the buckling load. It is believed that this type of buckling would be stable, whereas unstable buckling is observed.

5. The cross-sectional shape of the steel tape measure from which the tape springs used in the experiments had been cut is not perfectly circular, the edges are flat. The more accurate representation of the cross-sectional shape shown in Figure 1.6 gives $I = 4.67$ mm^4. This is only slightly different from the value found for the circular cross-section, 6.16 mm^4, and would not on its own account for the differences between theoretical and practical results.

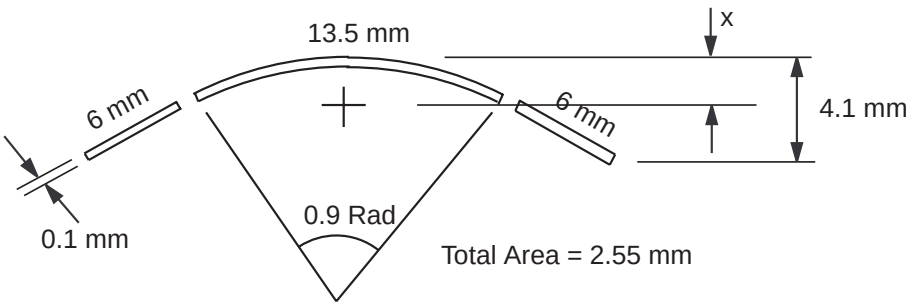

Figure 1.6: Cross-section of tape spring.

The pronounced curvature that is observed in the compression tape spring a long way before it buckles clearly indicates that this element is in bending as well as compression. This is due to the fact that the end blocks are offset from the centroid of the tape spring.

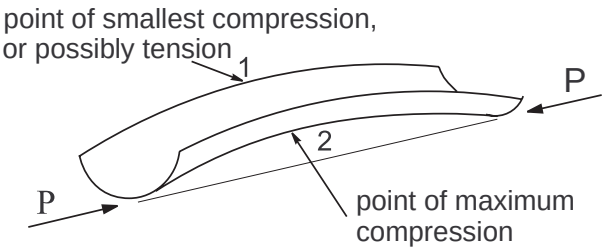

Figure 1.7: Buckling of compression tape spring.

Hence, to obtain a more accurate estimate of P_{cr}, The stress at points 1 and 2, defined in Figure 1.7, will be compared with the local shell-buckling values, which are determined as follows.

Local shell-buckling at point 1: Allen and Bulson (1980) gives the following expression for the critical stress in a rectangular plate

$$\sigma_{cr} = \frac{k\pi^2 E}{12(1-\nu^2)} \left(\frac{t}{b}\right)^2 \tag{1.8}$$

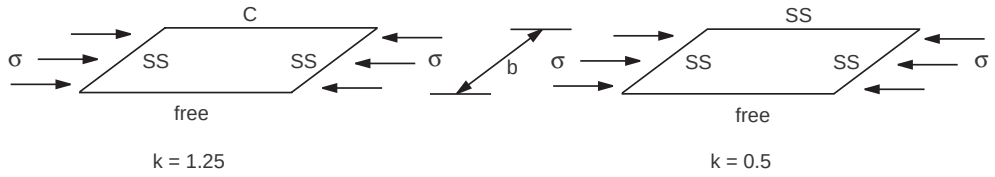

Figure 1.8: Values of k for different boundary conditions (from Allen and Bulson 1980).

Two different values of k have been considered, see Figure 1.8. The smallest value for b is the width of the flat edge of the cross-section, 6 mm, and the maximum value is half the arc-length, 12.7 mm. The flat edge has a free side and therefore $k = 0.5$ whereas for half the arc length $k = 1.25$. Substituting these values into Equation 1.8 gives a minimum value of $\sigma_{cr1} = 5.9$ N/mm^2 and a maximum value of $\sigma_{cr1} = 26.4$ N/mm^2.

Local shell-buckling values at point 2: Timoshenko and Gere (1961) states that a simply supported cylindrical panel buckles under the compressive load:

$$\sigma_{cr} = 0.6\frac{Et}{r} \tag{1.9}$$

For the values of t and r (thickness and radius respectively) given, Equation 1.9 gives a value of $\sigma_{cr2} = 840$ N/mm^2. [2]

Stress at points 1 and 2: In general,

$$\sigma = P\left(\frac{1}{A} + \frac{wy}{I}\right) \tag{1.10}$$

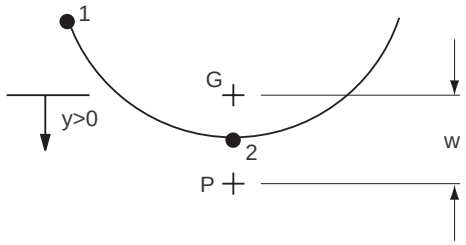

Figure 1.9: Definition of y.

Where y is the distance from the neutral axis and w is the eccentricity of P, defined in Figure 1.9. w is the central deflection of an eccentrically loaded strut, see Figure 1.10, given in Bazant and Cedolin (1991)

$$w = e\ \sec\left(\frac{\pi}{2}\sqrt{\frac{P}{P_E}}\right) = \frac{e}{\cos\sqrt{\frac{PL^2}{4EI}}} \tag{1.11}$$

[2]Timoshenko and Gere state that for approximately square, shallow panels this formula gives results that agree well with practical results. Because in this case the maximum stress occurs only at point 2, this critical stress can be taken to be accurate.

where e is the eccentricity of P at the ends of the strut, see Figure 1.10.

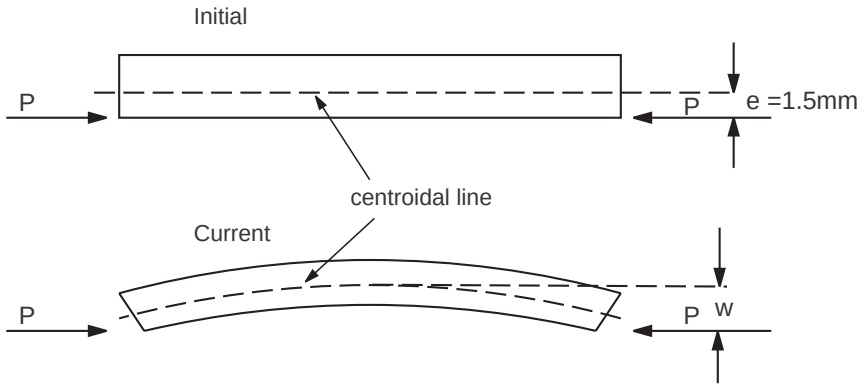

Figure 1.10: Eccentricity.

It turns out that for the range of hinge properties that we are analysing σ_{cr} at point 1 is negative, i.e. tensile, and hence the critical buckling stress cannot be reached at this point.

The stress at point 2 is compressive and therefore, combining Equations 1.10 and 1.11 and noting that $y = e$ for point 2, the buckling condition becomes:

$$\sigma_{cr2} = P_{cr}\left(\frac{1}{A} + \frac{e^2}{I\cos\sqrt{P_{cr}L^2/(4EI)}}\right) \tag{1.12}$$

Since σ_{cr2} can be found from Equation 1.9, the only unknown in this equation is P_{cr}. For the particular tape-spring properties that have been considered above, Equation 1.12 becomes

$$P_{cr}\left(\frac{1}{2.55} + \frac{1.5^2}{4.67\cos\sqrt{P_{cr}L^2/(4\times 210000\times 4.67)}}\right) = 840 \tag{1.13}$$

This equation has been solved iteratively for different values of L, using Matlab, and the results have been multiplied by $h = 18$ mm and then plotted in Figure 1.11, assuming a knock-down factor on the critical buckling load of 0.8.

It can be seen that: (i) increasing the length of the tape springs within the hinge quickly reduces the value of M_{max} and (ii) predicting M_{max} from Equations 1.1 and 1.13 is very accurate.

As a final test of the design equations that have been derived in this section, note that from Equation 1.1 there is a linear relationship between M^{max} and the tape spring separation h. This relationship has been plotted in Figure 1.12 along with a series of finite-element predictions and an experimental result. This plot confirms, again, the accuracy of the design equations that have been proposed.

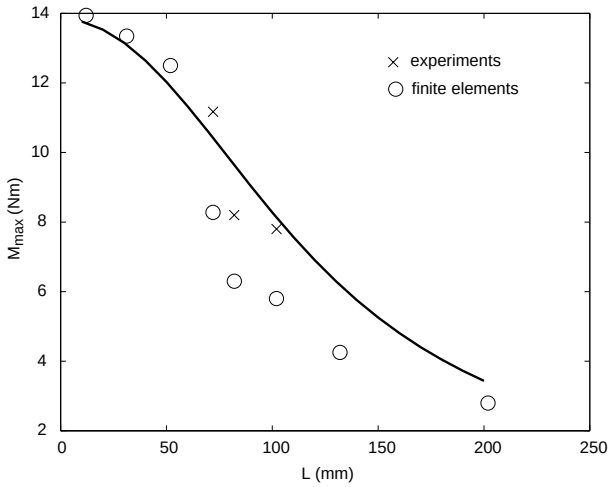

Figure 1.11: Comparison of Equations 1.1 and 1.13 with experimental and finite-element results.

1.5 Hinge Design

1.5.1 Conceptual Design

In order to gain an appreciation for the design and manufacture of "Rolamite" hinges (Chironis and Sclater, 1996) their connection to carpenter tapes a number of simple prototypes were built.

Initial Prototype

The main body of this model was constructed from wooden blocks with curved ends and two steel strips nailed to the sides. A tape-spring hinge was attached to the side of the model using two wood screws on either end. The shape of the wooden blocks was decided by drawing the path plotted out by one end of the tape-spring hinge when the other end was clamped. It was found that making the mating surfaces semi-circular with the hinge slightly offset from centre would produce a hinge which provided an opening path for the tape-spring hinge that was very similar to that drawn. A radius $r = 20$ mm, a hinge length $L = 150$ mm and a separation between blades $h = 15$ mm were chosen.

The main problem encountered with this initial design was that the two strips did not prevent the blocks of wood from rotating relative to each other and opening out.

Second Prototype

The initial prototype was modified by replacing the two steel strips with three strips of spring steel. The centre strip was made to be approximately twice the width of the other strips. Tensioning the strips proved difficult as they had to be held taught and then nailed into place.

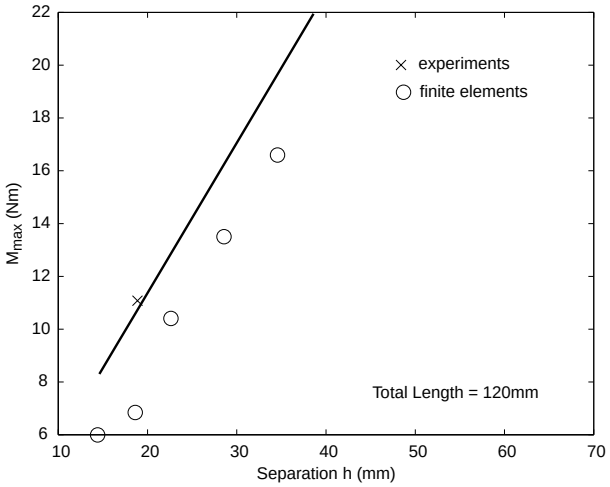

Figure 1.12: Further comparison of Equations 1.1 and 1.13 with experimental and finite-element results.

Considering the low quality manufacture of this hinge, it performed very well. The hinge opened and closed smoothly with high stiffness in all opening positions.

The connection of the tape-spring hinge to the Rolamite hinge was not sufficiently stiff to cope with the forces without any movement. On further examination it was found that the forces were all in the direction parallel to the tape. It was thought that the forces which caused this movement were due to the fact that the opening path of the rolamite hinge caused the distance between the tape connections to increase. This meant that either the tape-spring hinge would have been subjected to large strains or the supports would move.

The position of the tapes was modified so that they were offset to one side of the hinge. This made the hinge work without any movement of the connections when opening in one direction. When the hinge was opened in the other direction serious damage occurred to the hinge / tape connection. This is because if the tension tape is far from the centre of the hinge it undergoes severe tension.

Rotation above 180 degrees

One of the applications that is being proposed for the new self-locking hinge requires it to rotate through an angle of more than 180 degrees. In these models contact of the main body of the hinge prevents further rotation and so by changing the shape of the body it should be possible to gain rotations above 180 degrees. When the hinge is in the 180 degree position the two ends of the carpenters tape are separated by a distance of around 37 mm. The angle could be increased up to the point where the ends of the carpenters tape touch. On the model as designed this could be increased to an angle of around 210 degrees. Further angles would require a change in the length of the tapes.

1.5.2 Initial Design

Choice of Dimensions

The first stage in the design of a hinge utilizing tape springs is to decide the size of the springs; actually, the only choice available is the length of the spring because varying the other properties would require abandoning the use of standard, off-the-shelf tape measure, and the position of the two springs. The length and separation of the tape springs determines the maximum moment (M_{max}), as discussed in Section 1.4.

The next consideration is the opening path that the hinge follows. This path can be considered as the path that would be drawn out during operation of the hinge if a pen was attached to one side of the hinge and the other side was prevented from translation or rotation. This path is determined by the cross sectional shape of the mating surfaces and the position of the "pen".

For simplicity of design and manufacture it was decided that only circular mating surfaces would be considered. This choice enables the path to be characterized by the following equations:

$$R_x = 2r\cos\theta + x(1+\cos 2\theta) - y\sin 2\theta \tag{1.14}$$

$$R_y = 2r\sin\theta + x\sin 2\theta + y(1+\cos 2\theta) \tag{1.15}$$

where θ is the angle between the x-axis and the contact point of the hinge and R_x, R_y, x, y, and r are as shown in Figure 1.13.

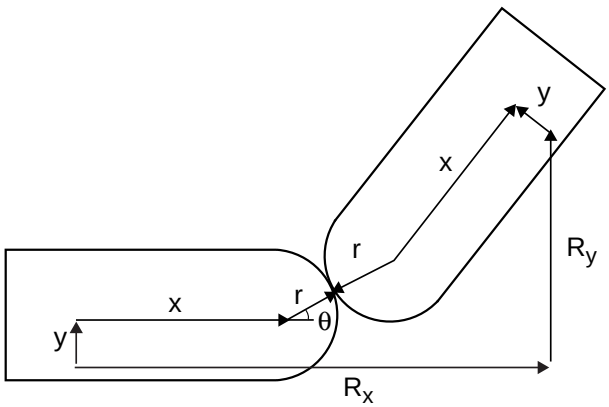

Figure 1.13: Kinematic properties of "Rolamite" hinge.

The most obvious constraint on the allowable values of x, y and r is the fact that the hinges are relatively inextensible. This means that the length of the hinge in any position ($\sqrt{R_x^2 + R_y^2}$) must not be significantly more than the original length ($2x + 2r$). However, note that a slight increase in the length when moved away from the deployed position will increase M_{max}. Another constraint is that the hinge should be as small as possible. This would suggest that as the length is fixed, r should be as small as possible.

There are three independent variables within this analysis; so, by fixing two and minimizing the third the optimum dimensions of the hinge can be found. In this case the folded separation distance of the outer springs $(2r+2y)$ and the length $(2x+2r)$ were fixed. The minimum value of r was found whilst keeping the length of the hinge in any position no more than the original length:

$$\sqrt{R_x^2 + R_y^2} \; < \; 2x + 2r \tag{1.16}$$

A second check was made into whether the outer hinge was capable of being folded into the 180 degree position. This check assumed that the minimum radius of curvature of the tape is the same as the transverse radius of curvature of the tape spring, as shown by Seffen and Pellegrino (1999). The following must then hold true:

$$s - 2r < L - \pi r_c \tag{1.17}$$

where s is the separation of the outer blades and r_c their transverse radius of curvature.

It should be noted that this analysis does not take into account all of the geometrical problems associated with the design of a hinge of this sort. For instance the interaction between the internal and external blades and whether the internal blade will have enough room to fold are ignored.

Previous experience suggested producing a hinge with length $L = 100$ mm and separation $s = 60$ mm in the 180 degrees folded configuration. A separation $h = 15$ mm between the tape springs was chosen. A Matlab program was written to solve the above equations and produced an opening path as shown in Figure 1.14 and the following dimensions: $r = 28.1$, $x = 21.9$, and $y = 1.9$ mm.

The hinge was designed with these values although it was later discovered that the small increase in the length of the tape was too large and caused the hinge to behave in an unpredictable manner. The value of y was then reduced to zero to counter this effect.

1.5.3 Detailed design version 1

A detailed hinge design was now produced using the dimensions found in Section 1.5.2. In this design it was decided that steel wires would be used instead of spring steel tapes. These would offer benefits in reduced hinge volume and simplified tightening.

Two Rolamite hinges were used, one attached to either side of the carpenters tape. This allows each hinge to have only two crossings of the wires. Although this set-up was found to be unstable in the prototyping stage, the joining of two of these unstable set-ups produces a stable hinge. A figure of eight configuration was chosen for wrapping the wires around the hinge allowing a simple tightening mechanism to tension each side of the hinge. Spiral grooves cut into the body of the hinge hold the wires restricting lateral movement of the hinge and preventing the wire from interfering with itself.

To ensure accurate and simple manufacture all parts were made from Aluminium alloy. The detailed design can be seen in Figure 1.15 and pictures of the as built hinge at a range of deployment angles are shown in Figure 1.16.

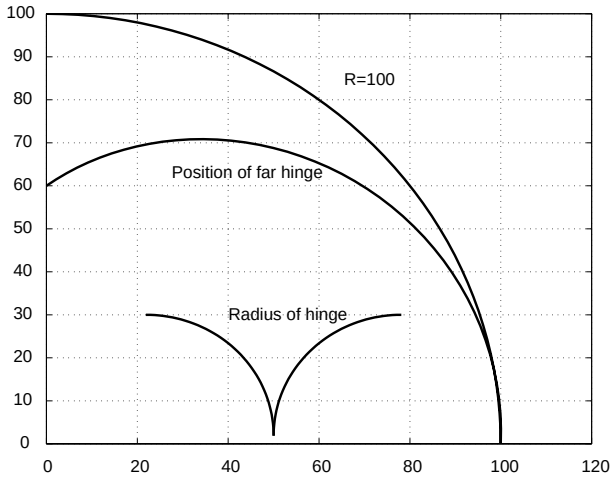

Figure 1.14: Initial design of hinge.

1.5.4 Stiffness

If the x-axis of the hinge is defined to be parallel to the tape springs and the axis of rotation of the hinge is defined to be the y-axis, here is how the hinge resists forces, F, and moments, M.

- $F_x^{>}0$: Contact of main body of hinge.
- $F_x^{<}0$: Tension in all wires.
- F_y: Shear of all wires, supported against side of grooves.
- F_z: Tension of half of the wires.
- $M_y = 0$: y is axis of rotation of hinge.
- M_x: Predominately tension of half the wires.
- M_z: Tension of half the wires and contact of the main body of the hinge.

Based on the above description of the modes of action of the hinge it is possible to estimate the stiffness and strength of the hinge in the above directions by substitution of the wire's dimensions, Young's modulus and strength.

1.5.5 Measurement of deployment moment

The deployment moment generated by the hinge was measured on an Instron materials testing machine. One half of the hinge was held in a chuck that could be rotated, whereas the other half of the hinge was held in a horizontal position by a vertical force from the Instron. The set-up can be seen in Figure 1.17 and the experimental procedure was as follows:

- Rotate hinge to approximately angle required.

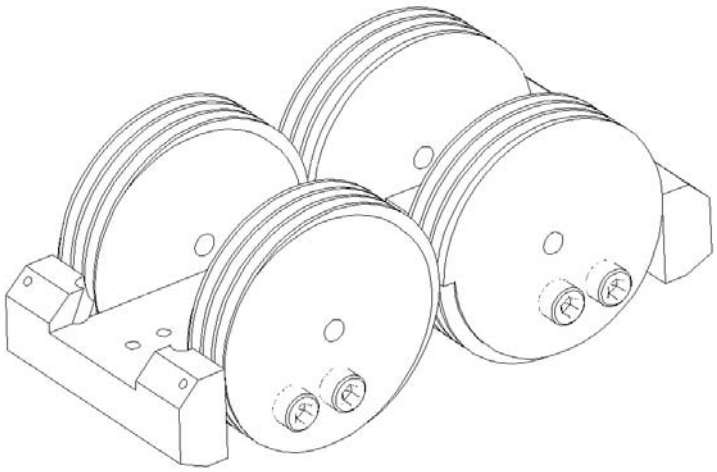

Figure 1.15: Detailed design of hinge version 1.

- Adjust height of Instron so that top part of hinge is horizontal (this is checked with a spirit-level).
- Move hinge so that force is applied through the correct point on the hinge.
- Measure force applied by Instron.
- Measure angle of lower hinge piece from horizontal.

The moment developed by the hinge can be found by multiplying the force F measured by the Instron by the perpendicular distance to the zero-shear point, this is the point of contact between the two halves of the Rolamite hinge. The moment can then be found from

$$M_{test} = F(r\cos(\theta/2) + r) \tag{1.18}$$

The additional moment due to the weight of the hinge has to be considered. It can be found by multiplying the horizontal distance between the centre of gravity of the hinge and the zero-shear point by the weight of the upper hinge part.

The mass of half the hinge is $m = 287$ g and its centre of mass was found analytically. Hence, the moment due to gravity can be estimated as:

$$M_{grav} = 9.81m(x_{-} + r\cos\theta/2) \tag{1.19}$$

The moment produced by the hinge is therefore

$$M = M_{test} + M_{grav} \tag{1.20}$$

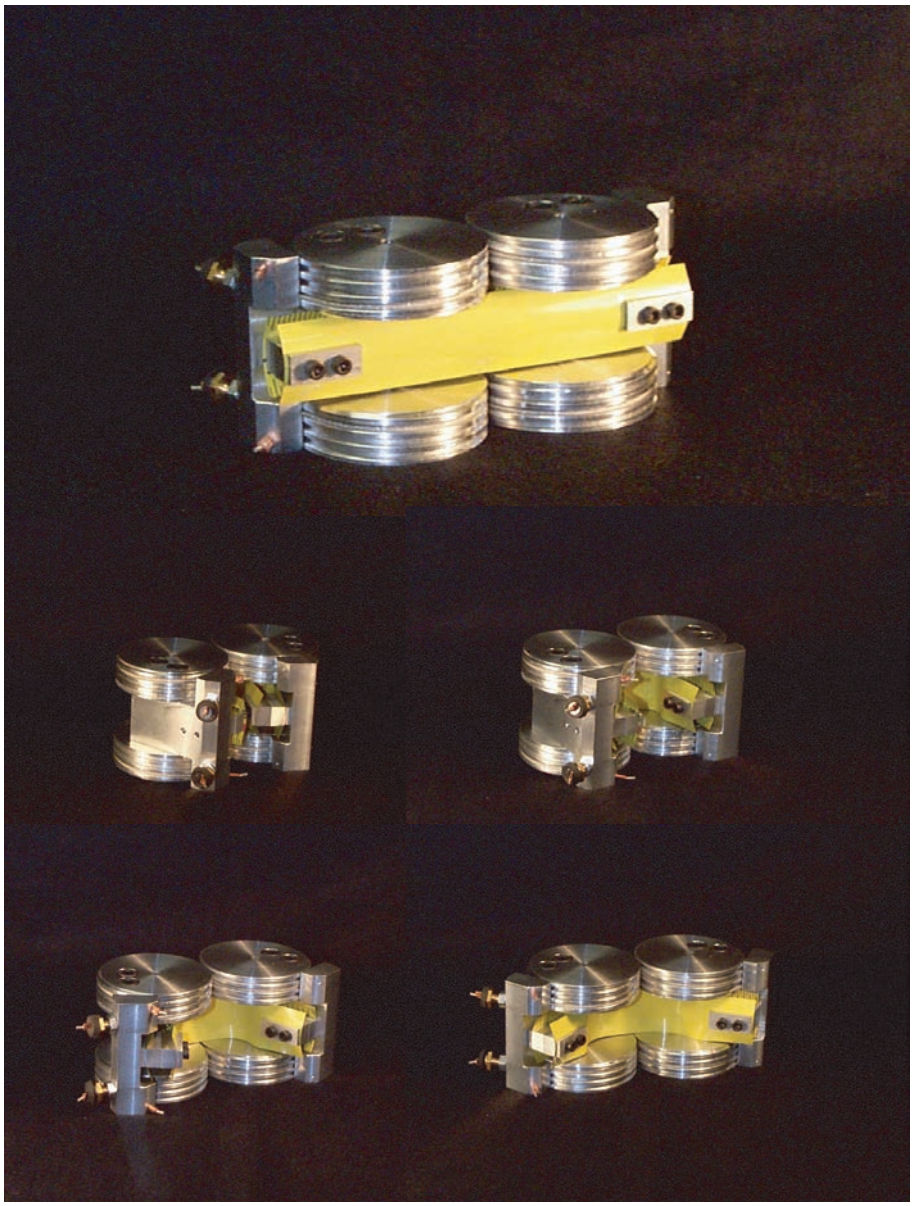

Figure 1.16: Various configurations of hinge version 1.

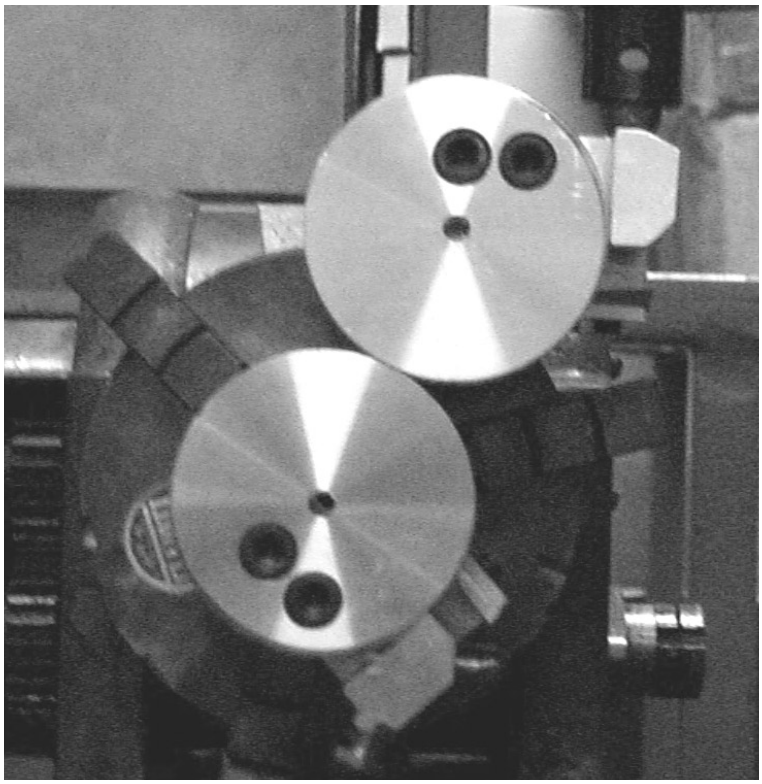

Figure 1.17: Experimental set-up for hinge version 1.

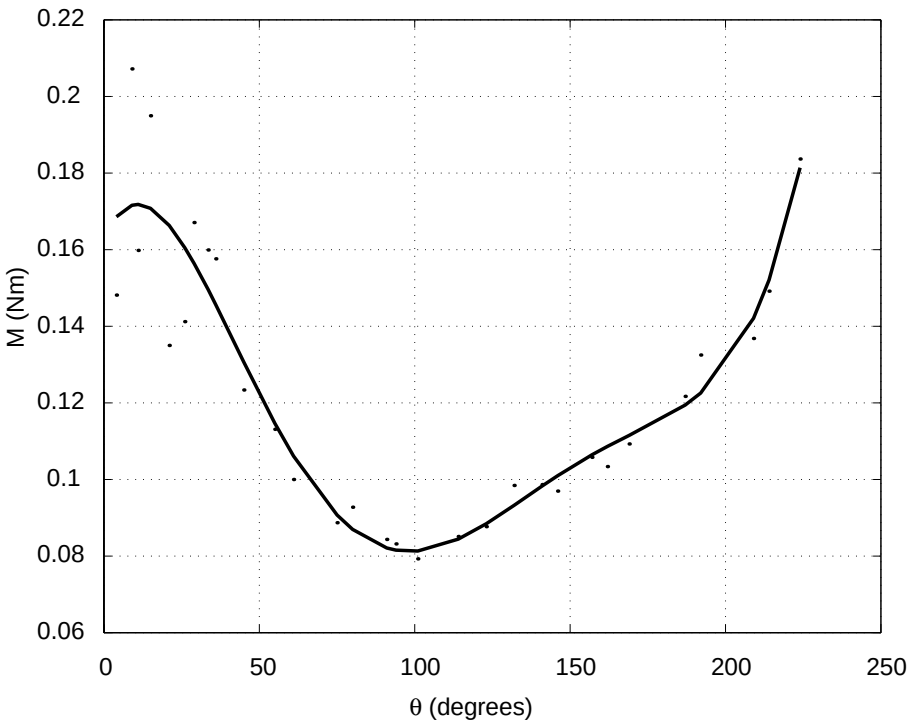

Figure 1.18: Moment-rotation relationship.

The relationship between M and the rotation angle θ can be seen in Figure 1.18. It can be seen that, as anticipated in Section 1.2, there is a large kick off moment at high values of θ, which decreases on opening (angle decreasing) and that near zero degrees (locking) the moment increases again. It can also be seen that below an angle of around 50° there is a large variation in the values of M. This is caused by the tape springs undergoing slight tensile strain which causes stable, low energy configurations to occur.

The effect of this was reduced by a redesign of the opening path, where the outer hinge offset, y, was reduced to zero. This was then tested with a double tape spring set up, with two compression and two tension springs. It can be seen from the results of this test, Figure 1.19, that the moment - rotation curve developed by this double spring hinge is different to that of the single spring hinge. The full rotation moment is around double that of the single spring hinge but the low values found around 50° to 100° are more than double those of the single spring hinge.

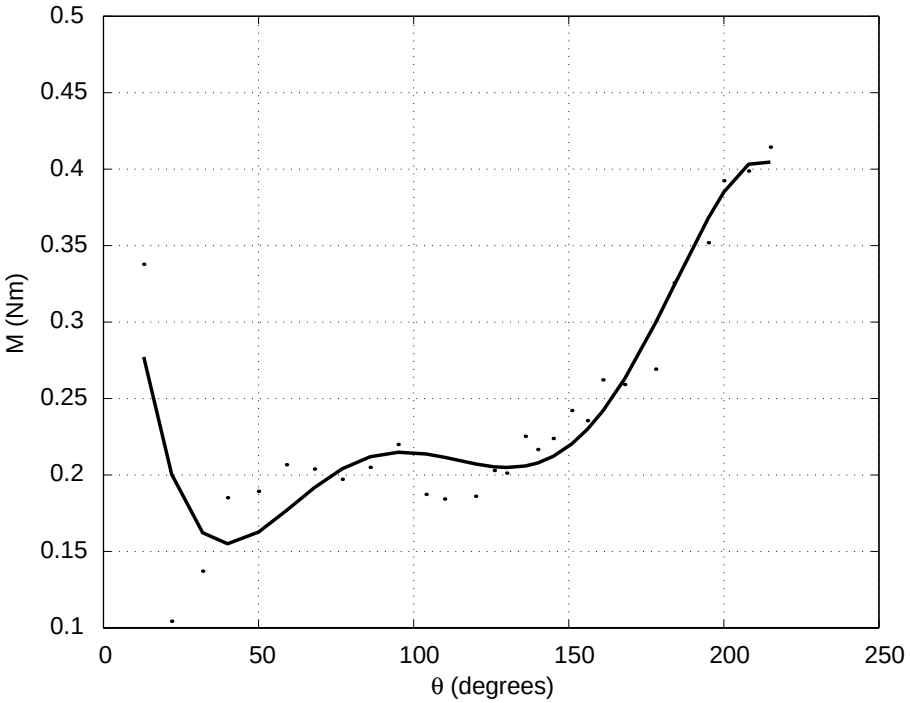

Figure 1.19: Moment-rotation relationship of redesigned hinge.

1.5.6 Detailed design version 2

The main problem with this design is the heavy weight ($\approx$ 600g). This has been addressed by a redesign where the volume of the hinge has been reduced to less than 20% of the original volume and a material change to Delrin, a space qualified acetal resin with a density of approximately half the density of Aluminium. These design changes resulted in an overall weight of 105 g, 16% of the original weight, which could be further reduced to around 60 g by replacing

more of the metal parts with plastic. This design can be seen in Figures 1.20 and 1.21. This redesigned version of the hinge performs well, although some twisting of the hinge could be seen.

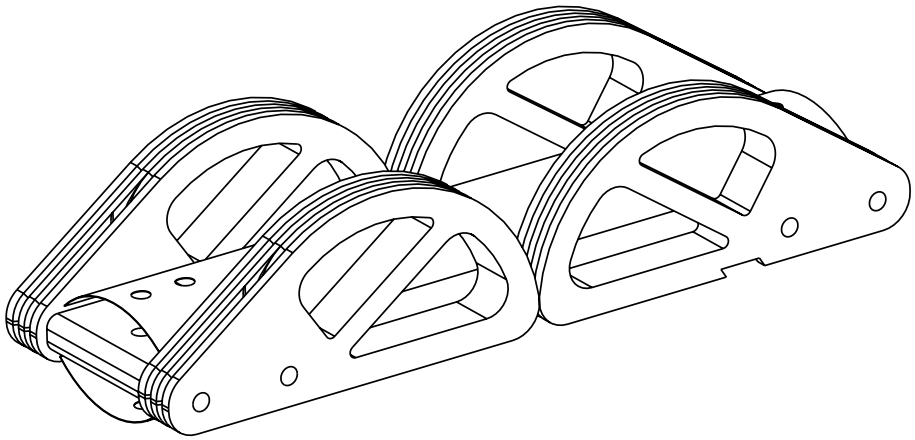

Figure 1.20: Detailed design of hinge version 2.

1.5.7 Conclusions

The hinge performed very well providing:

- Low friction operation, without the need for lubrication.
- Positive locking into the straight position.
- Kick off moment at first deployment.
- Simple assembly.

1.6 Recommendations for Further Work

Future analysis of designs of hinge of this type should examine a number of aspects:

- The prediction and control of the moment - rotation properties of the hinge should be improved. It was shown in this report that the addition of extra springs produced results that were not predicted. Ideally it should be possible to completely control the moment - rotation properties of the hinge. Likely methods for affecting this are to change the size, shape and number of carpenter tape springs or to add other springs.
- The controllability of the hinge is another important area for development. Space structures normally deploy very slowly over a matter of hours and for these hinges to provide this type of deployment some damping or external control method needs to be added.

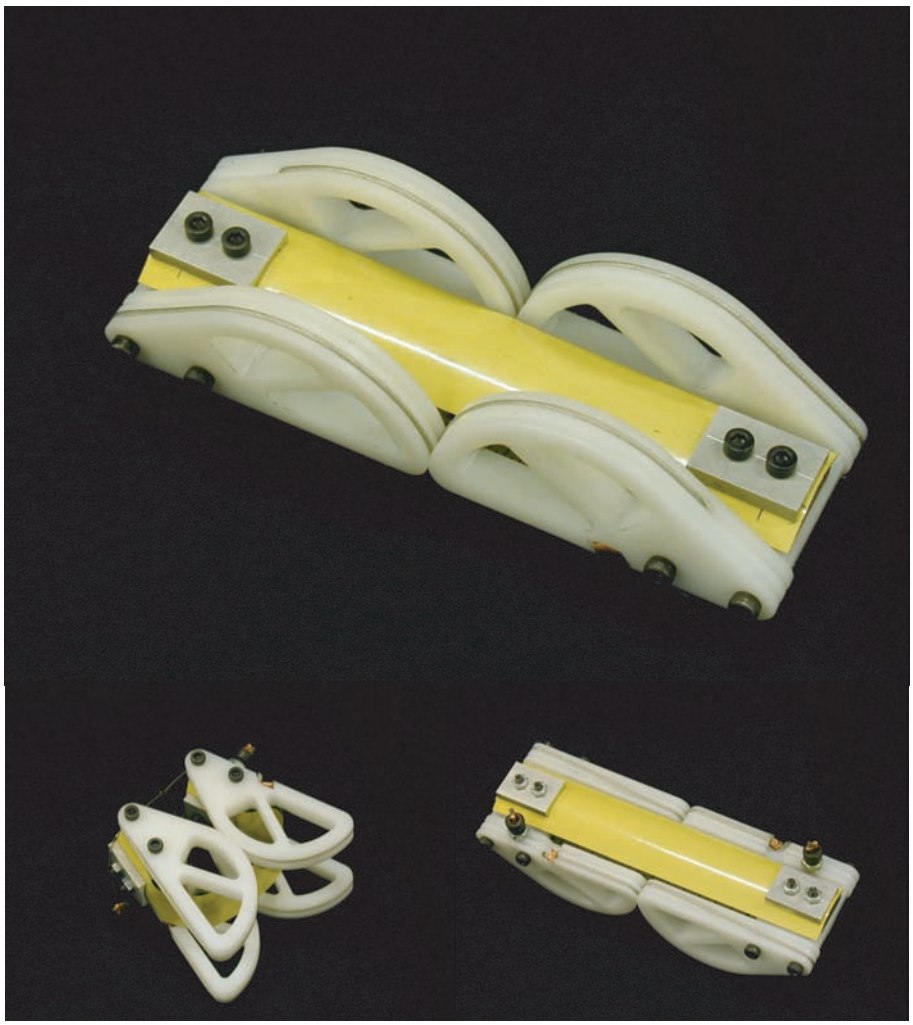

Figure 1.21: Two configurations of hinge version 2.

- The weight and performance of the hinge could be further improved by a detailed finite element analysis of the hinge parts. This would make it possible further optimise their design.
- The performance of the hinge with variations in temperature should be investigated.

Chapter 2

Conceptual Design of the Structure for a Deployable SAR

2.1 Introduction

Synthetic Aperture Radar (SAR) systems are used for a wide variety of tasks from mapping to environmental monitoring to military observation. The theory of operation of a SAR is complex and beyond the scope of this introduction, see Curlander and McDonough (1991) for more information, however one parameter that has an effect on the performance of a SAR is its size. The larger the SAR the better its performance. There is therefore pressure to make large SARs that can be packaged into as small a space as possible. This is at present mainly achieved by the folding of flat rigid panels. This chapter explores alternative techniques of packaging.

2.1.1 Previous Work

A new generation of low mass, low cost deployable L-band SAR systems are being developed at JPL (Lou et al. 1998). The SAR concept that has been developed at JPL is a roll-up inflatable frame of rectangular shape that supports and pretensions a flat membrane consisting of three-layers (radiator, ground, and distribution) separated by air (in space, vacuum). A description of this system, together with RF measurements taken from a 1/3 scale model can be seen in Lou et al. (1998). A photo of a demonstration model is shown in Figure 2.1.

This kind of technology can be realised without making recourse to inflatable systems, which are likely to be unsuitable for many potential applications. Hence, the aim of this study was to explore the potential of an alternative concept. This new concept is based on a rigid frame structure that is deployed by the elastic, self-locking hinges described in Chapter 1. This frame deploys and pretensions flexible membranes similar to those used in the JPL concept, and effectively replaces the inflatable element of the JPL SAR.

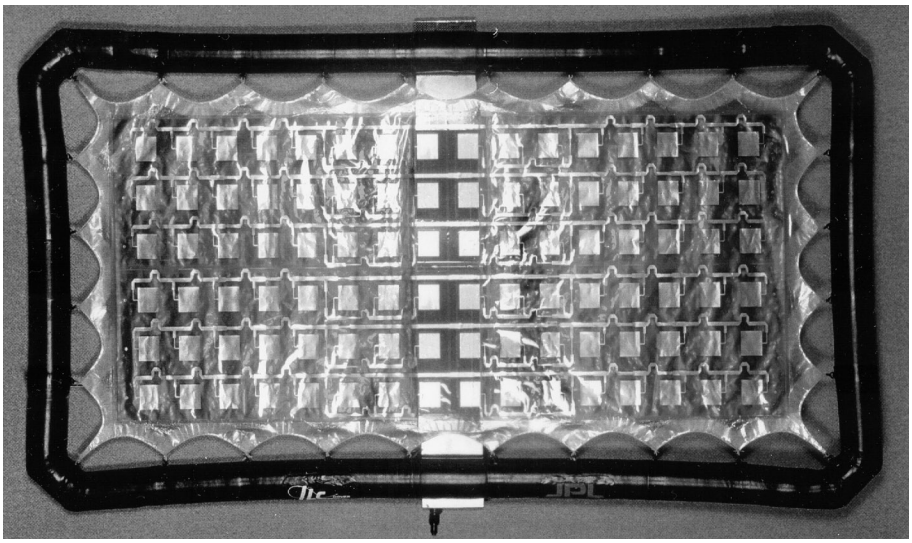

Figure 2.1: JPL inflatable SAR.

2.2 Size of SAR

A number of constraints due to the electrical design of the arrays are present in the sizing of the deployable sections. The eight arrays making up the surface are of a fixed size and each deployable section has to have a multiple of either two or three arrays on it. This leads to either a three array solution with two deploying sections 1.84 m by 0.75 m, plus a central section 1.22 m by 0.75 m or a four array solution with two deploying sections 2.45 m by 0.75 m and no central section. These array sizes can be seen in Figure 2.2.

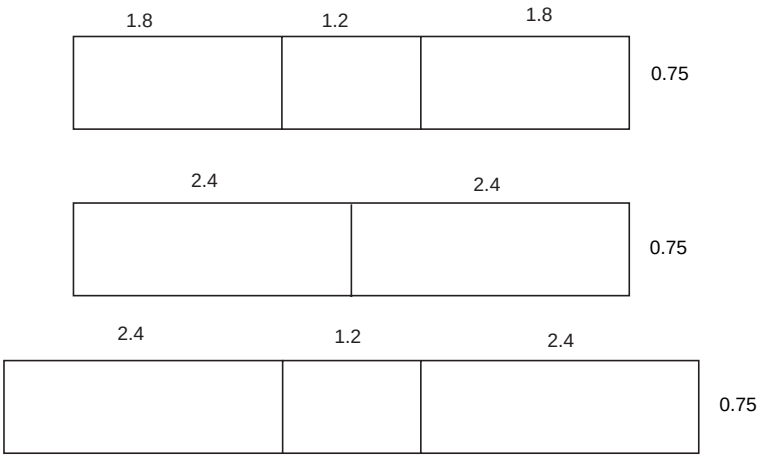

Figure 2.2: Sizes of SAR under consideration (dimensions in metres).

It should, however, be noted that the final solution that is taken to the next stage of design should be capable of both uniform and non uniform scaling, to be suitable for other design requirements.

2.3 Theory of Foldable Frames

This section is concerned with foldable frames that are made up of rigid bars connected together by hinges in a loop in such way that the frames can unfold from a compact bundle of bars to a square or rectangular framework.

An initial idealisation is to consider the hinges as being perfect revolute joints, which each have a single degree of freedom, and this section will consider what arrangement of bars and hinges will allow such an arrangement to fold and deploy.

In general, for a frame made up of n rigid bars, connected in a loop by n perfect revolute hinges, the overall *mobility* M, or number of freedoms of movement of the system, is given by

$$M = n - 6 \tag{2.1}$$

The ideal system would be one with $M = 1$, so there is only one possible folding/unfolding path. However, this implies that, in general, $n = 7$, and seven bars, connected in a loop by seven hinges, will be required. Clearly, this is unlikely to give a simple configuration.

However, Equation 2.1 is derived for the general case, and there are a number of special cases which allow a system to have $M = 1$ with fewer bars. Two examples of such systems will be introduced in this section, where symmetry considerations show that the systems have $M = 1$, even though both systems have $n < 7$. The first is a four-bar system which has been studied in some depth; the second is a six-bar system on which some initial work, including the manufacture of a simple model, has been carried out.

2.3.1 Four-bar frame

Figure 2.3 shows a simple model of a four-bar system folding from a square framework to a compact bundle of bars. The model is made from wooden bars connected together by revolute hinges. During folding, the model preserves two planes of symmetry, and one 2-fold symmetry axis; it is this special configuration that allows it to have $M = 1$. In fact, there are a family of similar solutions which keep this symmetry, and hence have $M = 1$.

The general configuration of the system when fully open is shown in Figure 2.4. The complete family of solutions that preserve the required symmetry are defined by varying the angle α from 0 to $\pi/2$. The particular model shown in Figure 2.3 had $\alpha = \pi/8$.

Figure 2.4 defines two sets of hinges, the θ-hinge on the 'outside' of the frame, and the ϕ-hinge on the 'inside' of the frame. Kinematics can be used to find the relationship between the rotation of these hinges as the frame unfolds.

Define θ as the rotation of the θ-hinge, and ϕ as the rotation of the ϕ-hinge in such a way $\theta = \phi = 0$ when the frame is full open (as shown in Figure 2.4), and $\theta = \theta_{\max}$, $\phi = \phi_{\max}$ when the frame is fully closed. $\theta_{\max}$ and $\phi_{\max}$ depend upon α.

For consistency across the graphs, it is convenient to define a 'closing parameter' Λ such that $\Lambda = 0$ when the frame is fully open and $\Lambda = 1$ when the

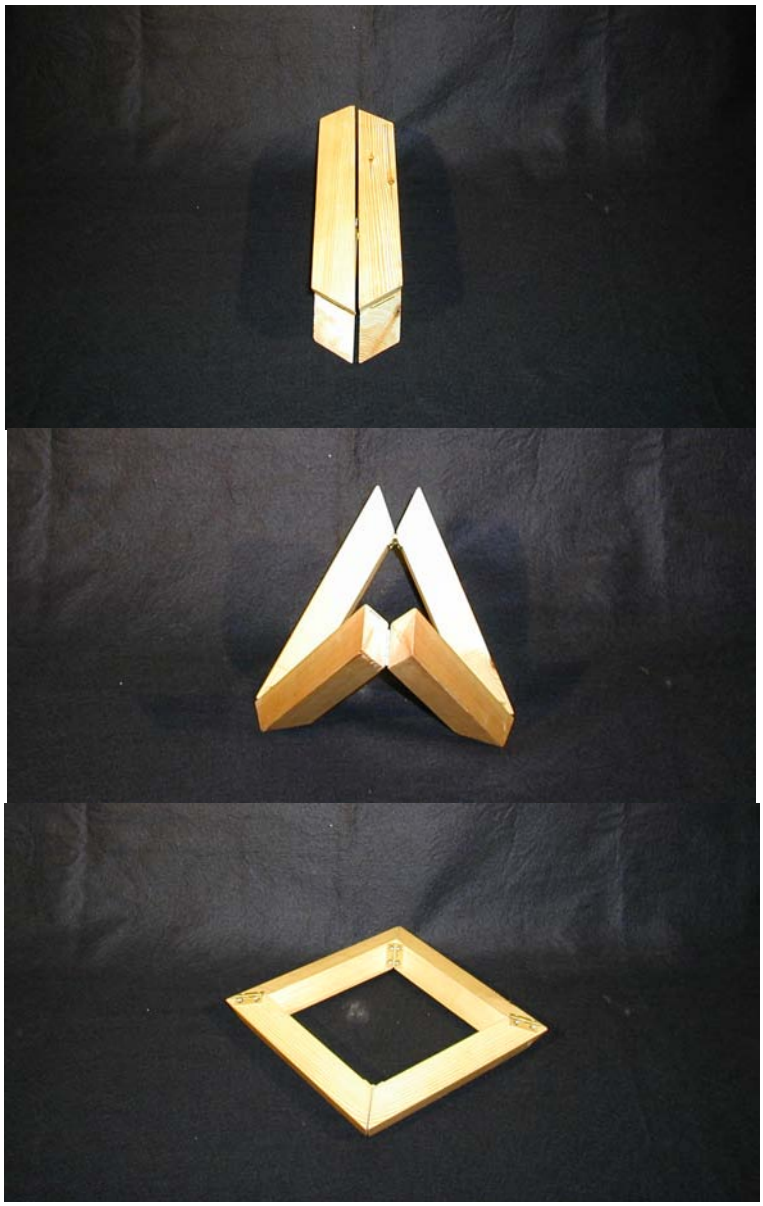

Figure 2.3: A model of the four-bar frame.

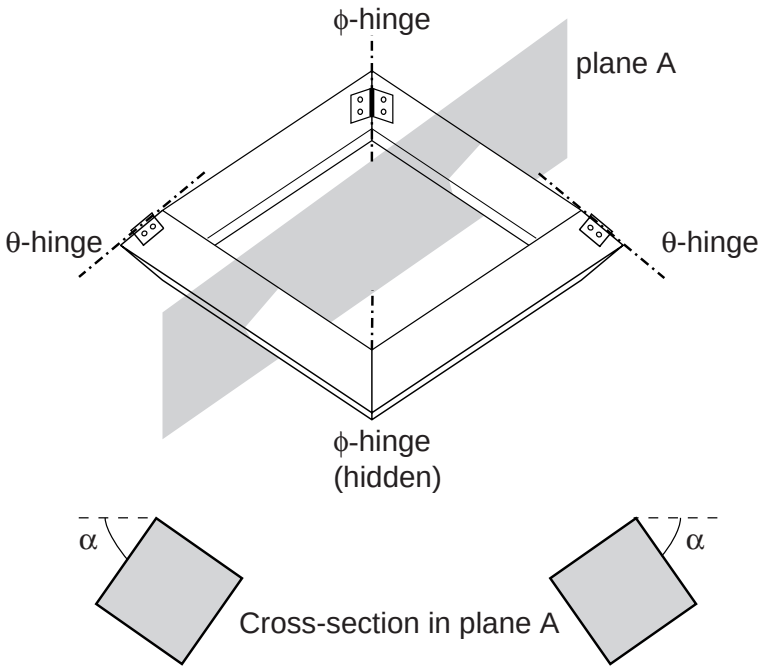

Figure 2.4: General configuration of four-bar frame.

frame is fully closed.

$$\Lambda = \frac{\theta + \phi}{\theta_{\max} + \phi_{\max}}$$

Figure 2.5 shows graphs of θ and ϕ against the closing parameter Λ for $\alpha = 0, \pi/16, \pi/8, 3\pi/16, \pi/4, 5\pi/16, 3\pi/8, 7\pi/16, \pi/2$. Figure 2.5 shows that for $\alpha = 0$ and $\alpha = \pi/2$, the closing of the structure is decoupled into two separate motions. For $\alpha = 0$, the structure initially folds around the aligned θ-hinges to the point where the two ϕ-hinges come together, and are aligned. The folding is then completed by folding around the ϕ-hinges. For $\alpha = \pi/2$, folding follows a similar pattern, but with folding initially around the ϕ-hinges.

For values of α greater than zero, but less than $\pi/2$, the folding about the two types of hinges is coupled. A measure of coupling would be to define a parameter C as

$$C = \min \left[\frac{\dot{\phi}_{\text{initial}}}{\dot{\theta}_{\text{initial}}}, \frac{\dot{\theta}_{\text{initial}}}{\dot{\phi}_{\text{initial}}} \right]$$

Figure 2.6 shows how C varies with α. It shows that the maximum coupling occurs when $\alpha = \pi/4$.

The ultimate aim of the frameworks that are being considered is to deploy a membrane. If the distance between two parts of the framework increases substantially, it will be difficult to attach the membrane to the frame. Figure 2.7 shows how the length across the diagonals of the framework vary as the frame

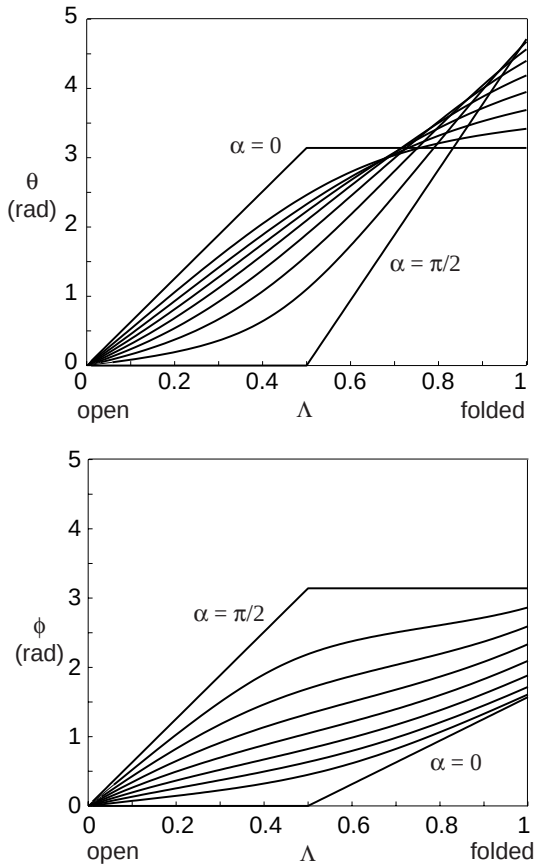

Figure 2.5: Hinge angles during the folding of four-bar frame.

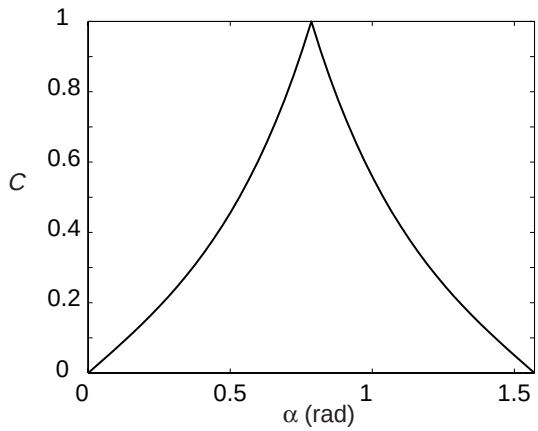

Figure 2.6: Coupling between hinge motions in four-bar frames.

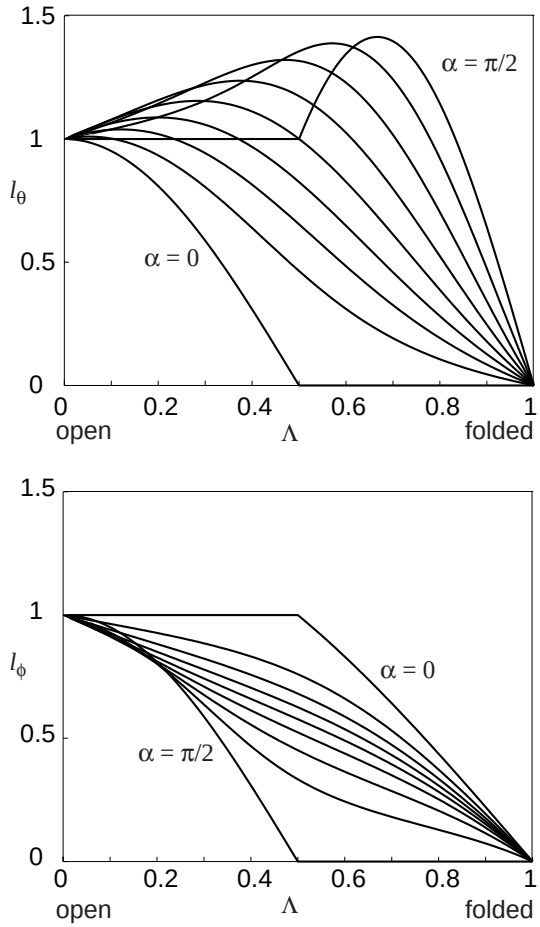

Figure 2.7: Diagonal non-dimensional lengths during the folding of a four-bar frame.

folds. l_ϕ is defined as being the ratio of the current length to the initial length between the two ϕ-hinges, and l_θ is defined as being the ratio of the current length to the initial length between the two θ-hinges.

Figure 2.7 shows that while l_ϕ is always less than or equal to one, l_θ has a maximum value that is always greater than or equal to one. To compare frames, it is useful to see the variation of the maximum value of l_θ, defined as $l_{\theta\max}$, with α, and this is shown in Figure 2.8.

An interesting point to note from Figures 2.6 and 2.8 is that, to a first order approximation, a small value of α introduces some coupling without changing $l_{\theta\max}$ from one.

2.3.2 Six-bar frame

An alternative foldable frame is shown in Figure 2.9. This shows a simple model of a six-bar system folding from a square framework to a compact bundle of bars. The model is made from wooden bars connected together by revolute hinges. During folding, the model preserves two planes of symmetry, and one 2-fold

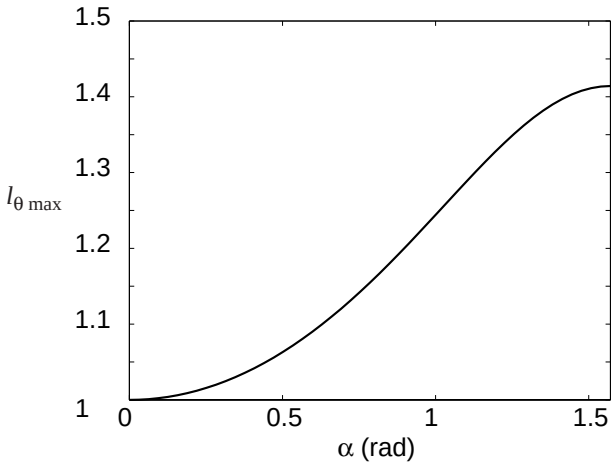

Figure 2.8: Maximum diagonal length during the folding of four-bar frames.

symmetry axis; it is this special configuration that allows it to have $M = 1$. In fact, there are a family of similar solutions which keep this symmetry, and hence have $M = 1$.

The general configuration of the system when fully open is shown in Figure 2.10. The particular model shown in Figure 2.9 had $\alpha = \pi/4$.

The kinematics of the six-bar foldable frame have not yet been studied. There is potential for this scheme to fold rectangular, rather than square frames. However, problems with the clashing of bars during folding, which do not occur for a square frame, will have to be overcome first.

2.4 Practical realisation of foldable frames

The structures described in the previous section can be realized using tape-spring hinges, and a membrane can be attached to the members of the frames. There are several ways of folding the membrane when the frame is folded. If the membrane is inextensional, in general, it is required that the attachments between the membrane and the frame be elastic. For example, Figure 2.11 shows a series of photographs of a square frame with tape-spring hinges (at 45° to the plane of the membrane) in the corners during deployment. In this model the membrane is a sheet of card that has been pre-creased to permit folding; it is attached to the frame through rubber bands.

For some particular hinge configurations the membrane can be rigidly attached to the frame as the diagonals of the square do not stretch when such configurations are folded.

Two ways of achieving the SAR configurations shown in Figure 2.2 have been considered. One approach is to divide up the required rectangular surface into two sets of foldable squares connected to a rigid element, which may be rectangular to achieve the prescribed dimensions of the SAR. A problem with this approach is that it poses significant constraints on the distribution of the TR modules of the SAR; also, the deployment of each frame needs to be con-

Figure 2.9: A simple model of the six-bar foldable frame.

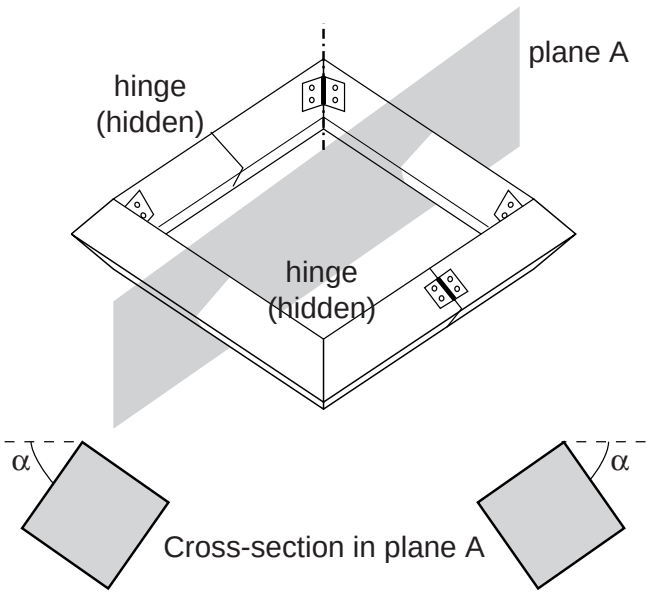

Figure 2.10: General configuration of six-bar foldable frame.

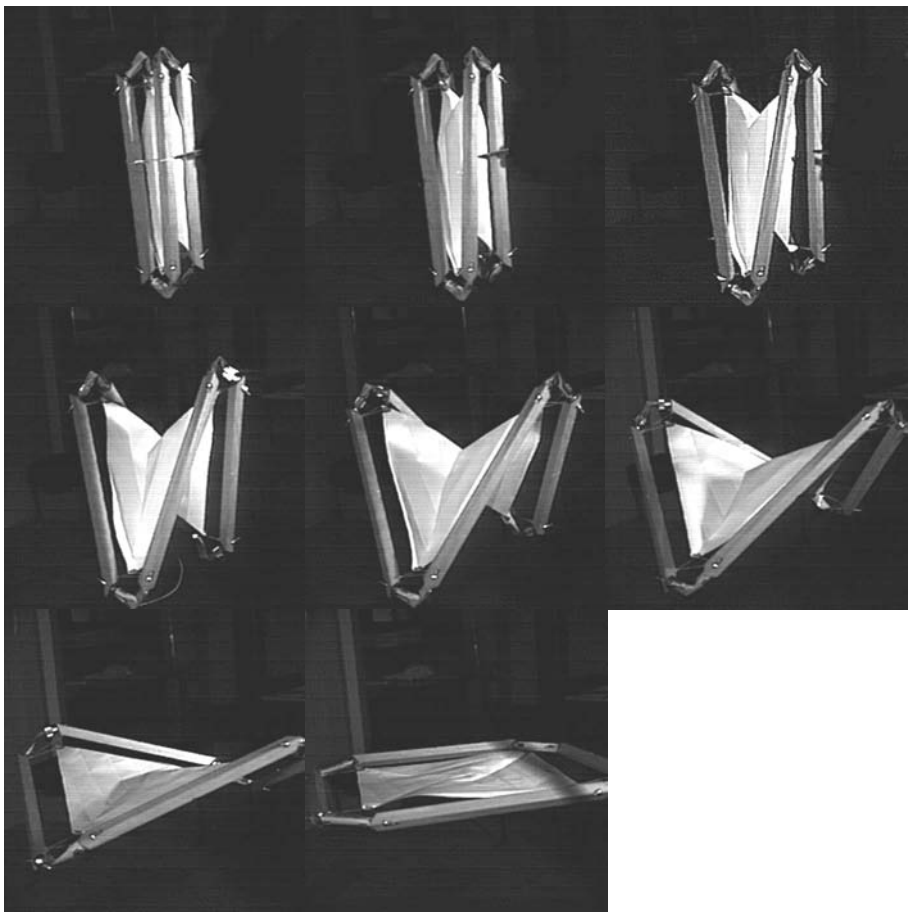

Figure 2.11: Square frame deployment - Time between consecutive frames 1/10 s.

trolled separately, which increases complexity. The alternative approach is to mount two rectangular frames on either side of a central element. This is the approach that has been investigated.

2.5 Rectangular Frames

A number of mechanisms for creating a flat rectangular surface from a flexible membrane were considered. In all of these mechanisms, as in the square frames described in Section 2.3, stiff beam elements connected by hinges were used to make a frame that could be folded into a compact structure. A preliminary analysis showed that two of these mechanisms were the most suitable and became the subject of further analysis.

2.5.1 Two-dimensional mechanism

The two-dimensional mechanism is a simple "lazy arm" mechanism with 6 single degree of freedom hinges, i.e. *revolute joints*, one at each corner and one in the middle of each of the long sides of the rectangle. This mechanism can be seen in Figure 2.12. In this version of this mechanism the longer sides have to be vertically offset to prevent collision when they fold across each other.

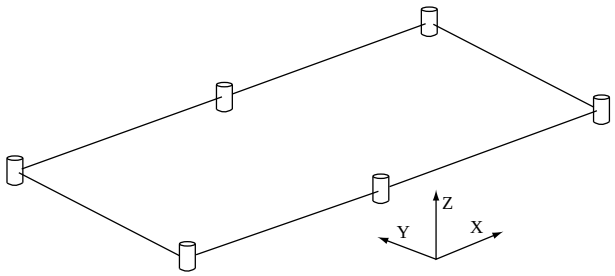

Figure 2.12: Two-dimensional mechanism.

2.5.2 Three-dimensional mechanism

This mechanism involves 6 revolute joints, one at each corner and one in the middle of each of the long sides of the rectangle. An example of this mechanism can be seen in Figure 2.13. The corner joints have their major axis rotated as shown in Figure 2.13. The nearest hinge, in this example, is in the direction (1 1 1) and the axes of the middle hinges lie within the plane of the frame, (0 1 0). This creates a mechanism where one of the long sides folds *upwards* out of the plane of the frame and the other *downwards*, thus avoiding the conflict inherent in the two-dimensional mechanism. When the frame is completely stowed the members all lie in the same plane next to each other.

If revolute joints are used within this model the mechanism will not function. For the mechanism to work extra degrees of freedom need to be added. There are a number of methods of adding extra degrees of freedom including:

- Using hinges with more than one degree of freedom.

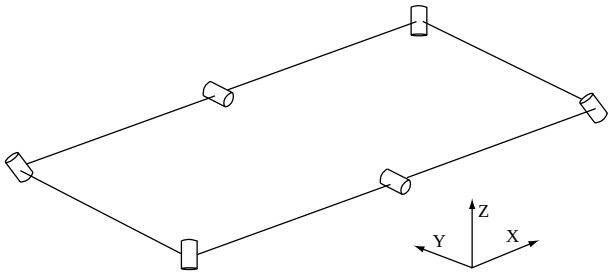

Figure 2.13: Three-dimensional mechanism.

- Using flexible members.
- Adding extra hinges.

These solutions are all considered in the next section.

2.6 Modelling of Mechanisms

A number of models of varying degrees of complexity have been made. The aim of these models is to show the validity of the proposed mechanisms, without necessarily being an indication of the final design solution. These models included physical models, made from wood and Aluminium with standard door hinges or tape spring hinges of varying complexity, and computer simulations of the mechanisms.

A suite of linked computer programs from Parametric Technologies (1999) were used to model the mechanisms in the following way:

- Three-dimensional models of the rigid elements comprising the mechanisms were created in the solid modeller, Pro/Engineer.
- These elements were joined together using a kinematic modeller, the mechanisms design add-on to Pro/Engineer. This allowed a number of simple connections of 1 to 6 degrees of freedom to be added quickly and simply, between parts or other mechanisms. The created mechanism can be dragged through its allowable range of motion in real-time. This dynamic dragging feature proved to be a very handy tool for predicting whether a particular mechanism would work, the number of degrees of freedom and in which way they acted and if the mechanism had been assembled correctly.
- The models were then imported into the dynamic modeller Pro/Mechanica. Here more complex joints such as gear connections could be added and by adding material properties, initial conditions and loadings full dynamic simulations made.
- The models and the dynamic results were combined into MPEG files (viewable on a webpage) with Pro/Flythrough, this also enabled zooms and pans to be added to the final MPEG.

2.6.1 Two-dimensional frame

A model of the lazy arm mechanism was made from wooden beam elements and standard door hinges. This model functioned well and a picture of it can be seen in Figure 2.14. It shows that there is one extra, unwanted, degree of freedom in the mechanism. This extra freedom is shown by holding one of the short arms fixed and rotating the other short arm about the z-axis (as defined in Figure 2.12).

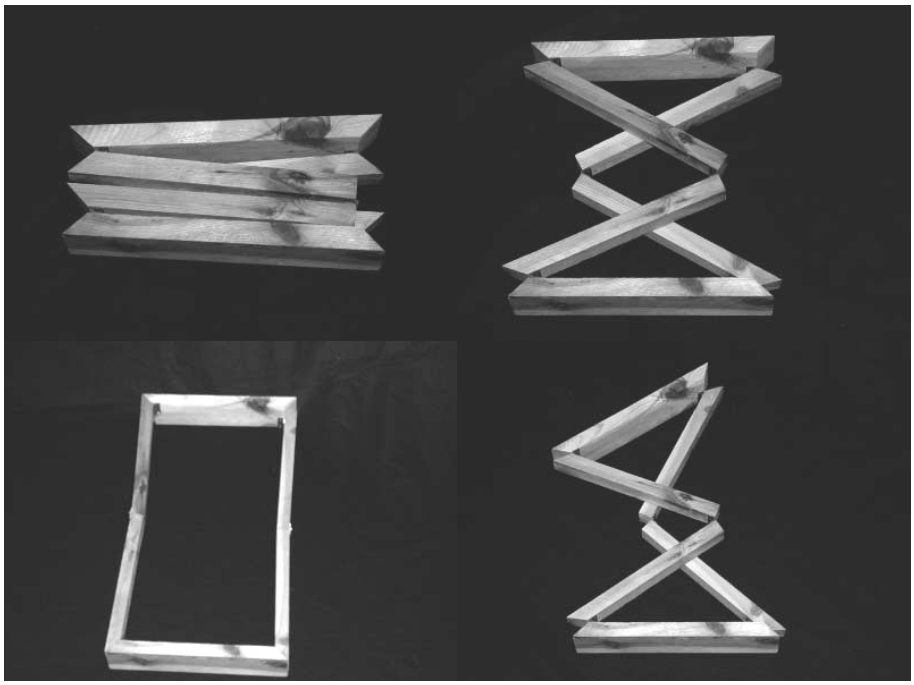

Figure 2.14: Lazy arm frame.

The results of a simulation of this mechanism can be seen in Figure 2.15. This simulation showed that the effect of this extra degree of freedom can be overcome by keeping all the forces on the model symmetrical. Such a symmetrical force loading is however much harder to achieve in real world situations. However, this frame is modelled without a membrane and the action of the membrane will tend to help restrict rotation around the z-axis.

2.6.2 Frame with 6 revolute joints

A number of variants of three-dimensional models were built and simulated in order to test new theories and designs. The first model had 6 revolute joints arranged as described in Section 2.5.2. These hinges were single degree of freedom door hinges that connected rigid wooden beam elements. This model did not function as a mechanism. This is because extra degrees of freedom need to be added to the model. A simple analysis was made to predict the error angle, defined in Section 2.6.5, and the results are shown in Figure 2.16.

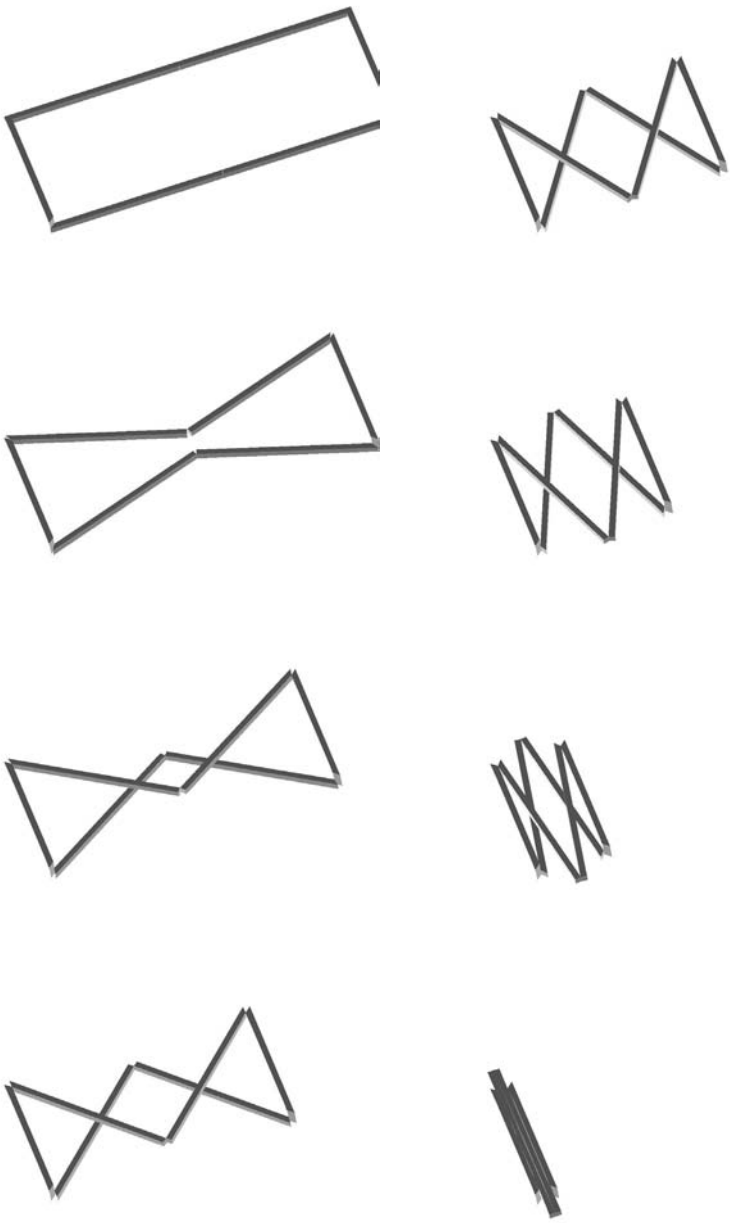

Figure 2.15: Simulation of two-dimensional mechanism.

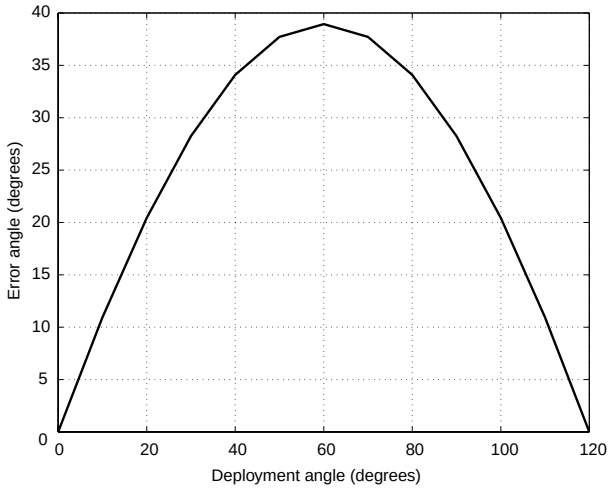

Figure 2.16: Error angle during deployment of frame with 6 revolute joints.

2.6.3 Frame with 8 revolute joints

The first attempt to create a working mechanism was to add extra hinges in the middle of the short sides of the model. The hinges in the centre of the long arms were also rotated as shown in Figure 2.17.

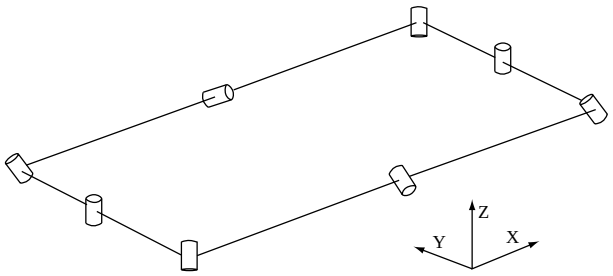

Figure 2.17: Frame with 8 revolute joints.

The main problem with this model is that in certain positions it locks up. Great care is required to avoid these configurations. This makes the mechanism unsuitable for space applications due to its low reliability and unpredictable nature. No simulation of this model was attempted.

2.6.4 Frame with 6 multi-degree-of-freedom hinges

A model of the three-dimensional mechanism described in Section 2.5.2 was built. This model used tape-spring hinges to provide both deployment actuation forces and stiffness in the deployed configuration. These hinges were manufactured by joining two tape springs next to each other as shown in Figure 2.18. This hinge has a predominant axis of rotation about the x-axis, defined in Figure 2.18, although rotation is possible also around the other axes.

A dynamic deployment test of this model was made. The heavy weight of the beam members and multiple degrees of freedom of the hinges necessitated

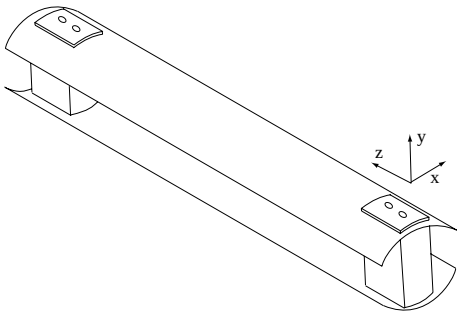

Figure 2.18: Coordinate axes for tape spring hinge.

the addition of a gravity compensation system, which required the frame to be suspended from wires attached to the centres of the four beam elements making the long sides of the frame. The mechanism was then folded into the stowed configuration and secured with an elastic band. This elastic band was then cut and the elastic energy stored in the hinges deployed the frame. A sequence of high speed camera pictures of this deployment can be seen in Figure 2.19.

It can be seen from the figure that the deployment of the frame does not occur in the controlled manner that would be desired because the hinges snap through the straight position a few times before locking. This is most likely due to the anti-gravity support system: it can be seen from examination of Figure 2.19 that the centres of gravity of the longer beams at the rear of the picture are considerably lower in the deployed configuration than in the stowed configuration. Hence, the potential energy of the frame decreases during deployment and this provides additional kinetic energy, which causes the hinges to snap through. A better zero-gravity system will need to be developed to avoid this; an alternative is to slow down the deployment of the frame, by controlling the deployment speed or by damping.

It was decided that one of the simplest ways of removing the snap-through problem was to control the deployment. A membrane was attached to the frame at one of the short ends and to a motorized roller attached to the other end. A Mylar membrane was attached to the frame by elastic bands and glued to a motorized roller system that had been bolted to the frame. The frame was then folded into the stowed condition and the membrane rolled up around the roller. By unrolling the membrane, control of the frame deployment could be achieved. However, with the use of multiple degree of freedom hinges throughout the frame the membrane constraint was not enough to fully constrain deployment. Some degree of constraint of the mechanism was achieved by adding two more wires to the uppermost corners of each of the short arms of the frame. The tension of these wires was controlled by a human operator.

Pictures of a deployment constrained in this way can be seen in Figure 2.20. It can be seen by looking at the first frame in the sequence that the frame is still not fully constrained, although sufficient constraint has been applied to control the deployment speed of the frame.

No simulation was made of this model, due to the difficulty of prescribing degrees of freedom for the hinges without making the simulation behave

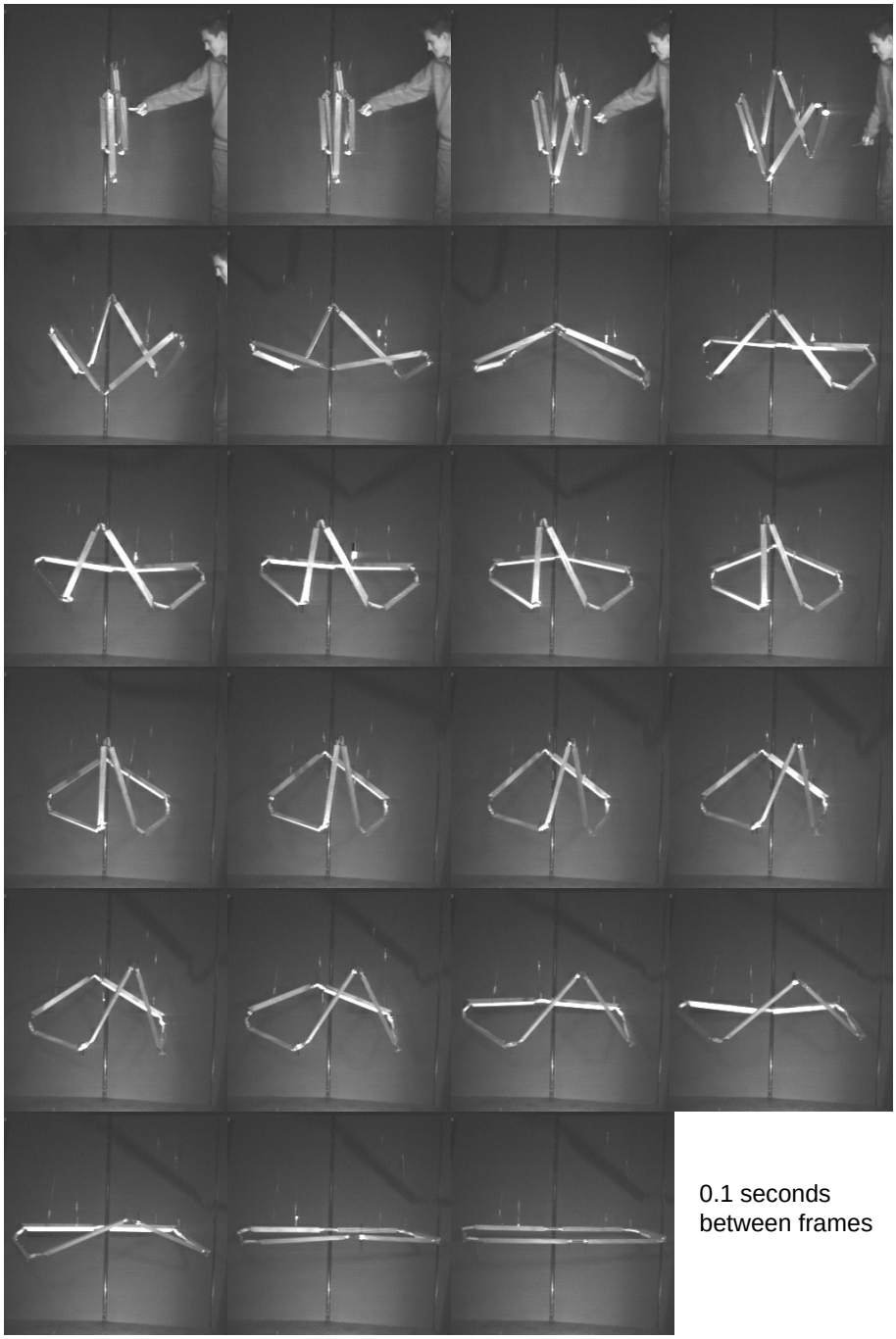

Figure 2.19: Deployment test on frame with 6 tape-spring hinges.

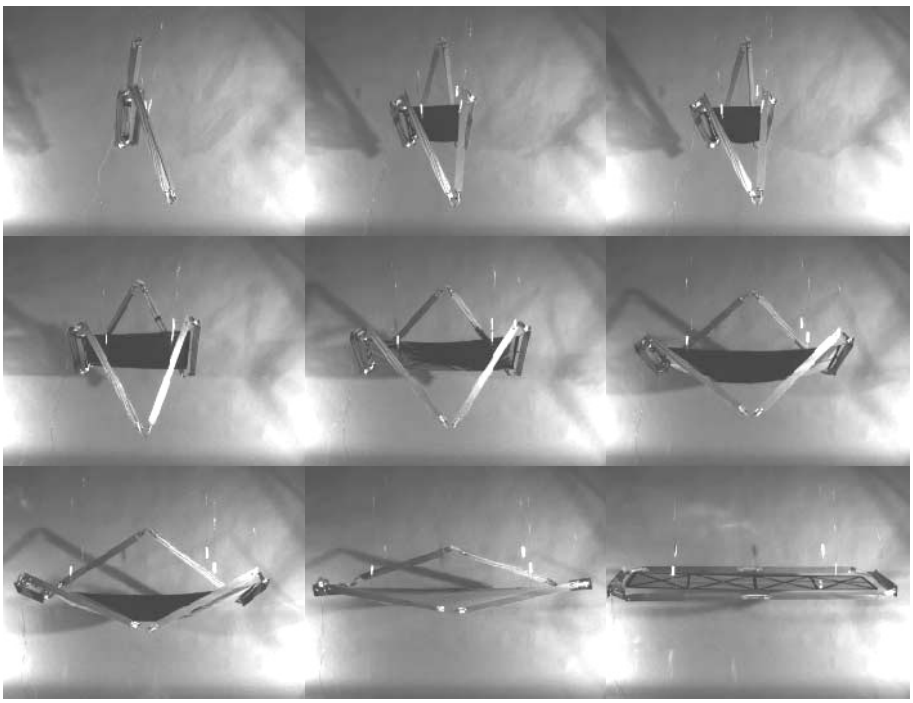

Figure 2.20: Membrane-constrained deployment of frame with 6 tape-spring hinges.

erratically.

2.6.5 Frame with 4 revolute joints and 2 flexible hinges

The next development was to use revolute joints at the corners of the frame and multiple degree of freedom joints in the middle of the longer sides of the frame. In practice, the revolute joints would be realised with Rolamite hinges and the multi-degree-of-freedom joints with standard tape-spring hinges.

A number of simulations of this frame have been developed. In the first simulation all the corner joints were modelled as revolute joints and the remaining two as six degree of freedom joints. It had been found that if only rotational freedoms were allowed at all hinges the mechanism would not function; small translations within the two central joints were required to prevent the mechanism becoming numerically ill conditioned. The six degrees of freedom within these joints were constrained by elastic elements with one of the rotational stiffnesses much smaller than the others. The simulated deployment of this mechanism can be seen in Figure 2.21.

The x, y and z axes for the simulation are fixed to one of the members, as follows. The y-axis is co-axial with the members and the x-axis is orthogonal to y and at a specified angle to the revolute joint at the other end of the member, see Figure 2.22.

The simulation of this set up showed that, if a true ball joint was used, the rotations about y and z, θ_y and θ_z reach peak values of nearly 35°, Figure 2.23.

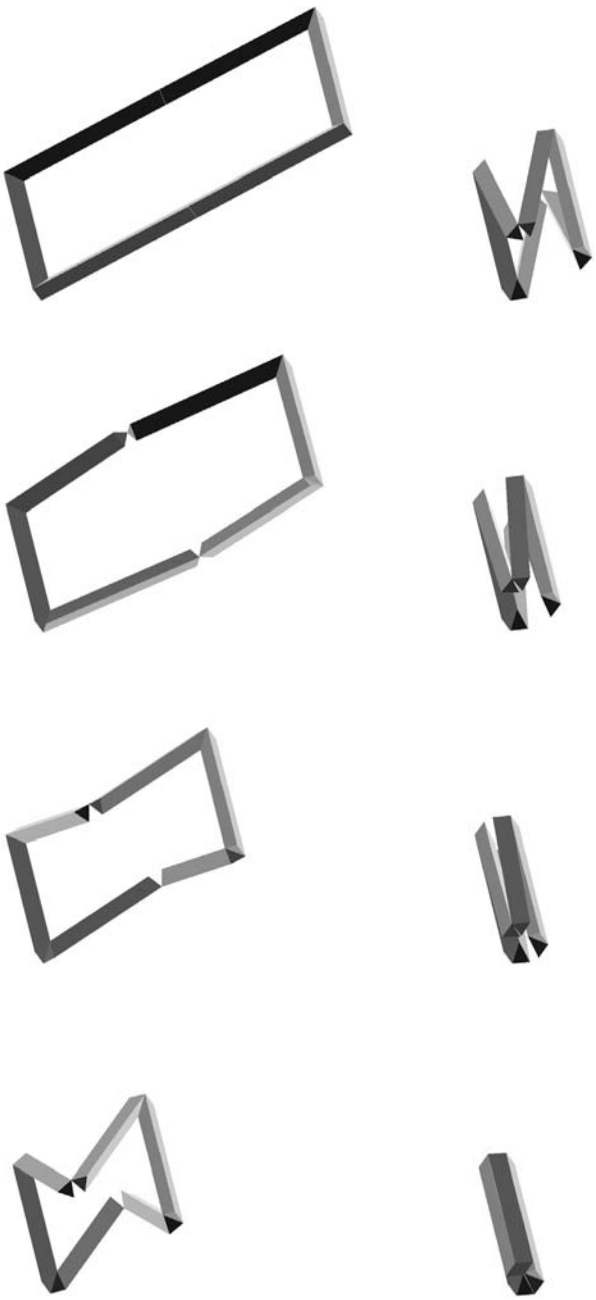

Figure 2.21: Simulation of frame with 4 revolute joints and 2 flexible hinges.

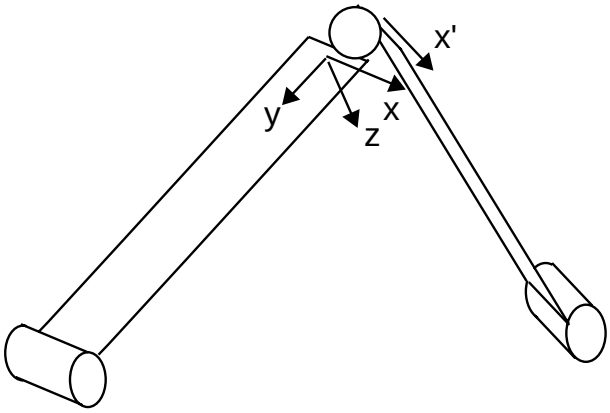

Figure 2.22: Definition of coordinate system.

The angle between the x-axis and the corresponding axis, x', on the other member is defined as the *hinge error angle*, θ. The hinge error angle can be calculated from

$$\theta = \cos^{-1}\left(\cos\theta_y \times \cos\theta_z\right) \tag{2.2}$$

and a plot of θ against against the x-axis rotation, θ_x, can be seen in Figure 2.24, this is exactly the same result found from the analysis of Section 2.6.2. Note that θ goes up to $\approx 40°$ and for the frame to deploy without damage it must be ensured that the hinge design allows such an error without damage.

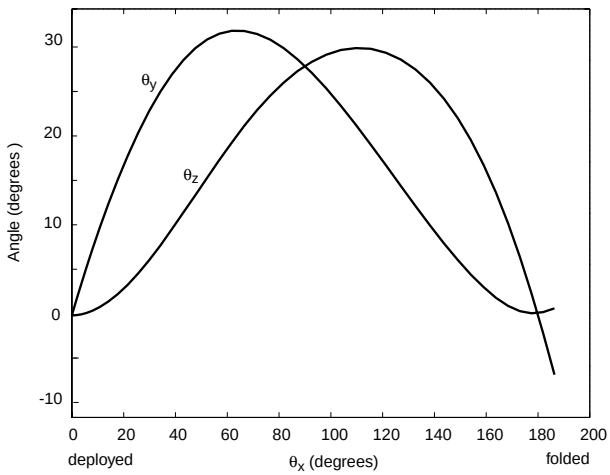

Figure 2.23: Components of rotation of central hinge, from Pro/Mechanica.

The tape-spring hinges presented in Chapter 1 do not, however, behave exactly like revolute joints. A better model for these hinges can be constructed by defining two spur gears whose rotation axes are attached to a connecting member. This was achieved in Pro/Mechanica by solidly connecting two cylindrical sections, co-axial with and of the same radius as the contact surfaces of the Rolamite hinge, and a connecting piece, all of zero mass and 100% transparency, to the hinge. The cylindrical sections were modelled as spur gears and

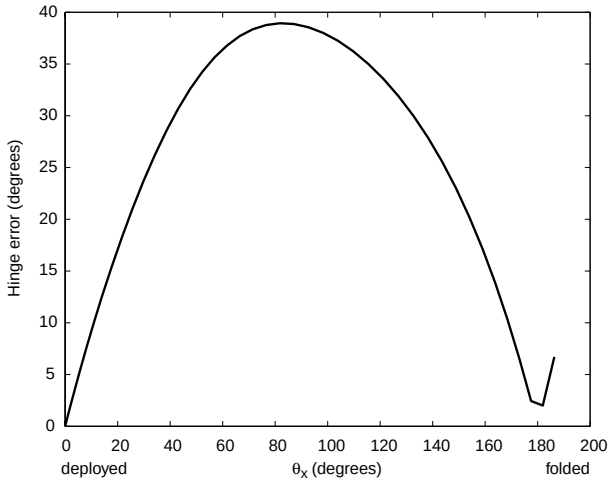

Figure 2.24: Hinge error, from Pro/Mechanica.

the connecting piece was attached via revolute joints to the axes of the contact surface. This model can be seen in Figure 2.25.

A simulation of the mechanism with the correctly modelled hinges at the corners and 6 degree of freedom joints in the middle of the long sides of the rectangles can be seen in Figure 2.26. This shows that even with the slightly different conditions of the real hinge the mechanism still works without any problems. The y and z components of the rotation of the middle hinge during deployment are plotted in Figure 2.27. Note that one of the two rotation components does not reduce to zero upon full packing of the frame.

A model of this frame mechanism is being constructed at present.

2.6.6 Frames with flexible members

An alternative to the frame with 6 revolute joints considered in Section 2.6.4 is to use torsionally flexible members for the long sides of the rectangle. This idea was investigated by setting up a mathematical model in which the hinge error angle —i.e. the angle between the two positions that the hinge would like to be in, assuming rigid side members— is resolved by twisting the two members. To achieve this, the members are required to have relatively low torsional stiffness, while retaining high axial and bending stiffness. This can be achieved with open-section side members. The end members need to be torsionally stiff, and hence closed section members would be used.

Figure 2.28 shows that a maximum twist angle of 45° in a side member occurs just before the fully-deployed configuration is reached. Initial calculations showed that a 45° twist in an Aluminium alloy angle with 25 mm wide flanges and a thickness of 0.56 mm would result in a maximum shear stress of 30 N/mm^2. This is less than one quarter of the yield stress. This member was then checked against buckling, assuming that an axial force of 200 N is required to prestress the membrane.

Note that in this frame the twist angle increases from 0 to 45° almost uni-

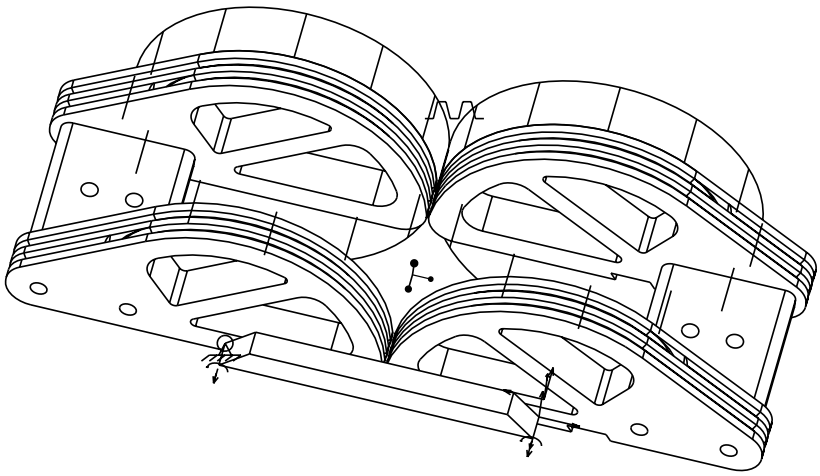

Figure 2.25: Pro/Engineer model of tape spring hinge.

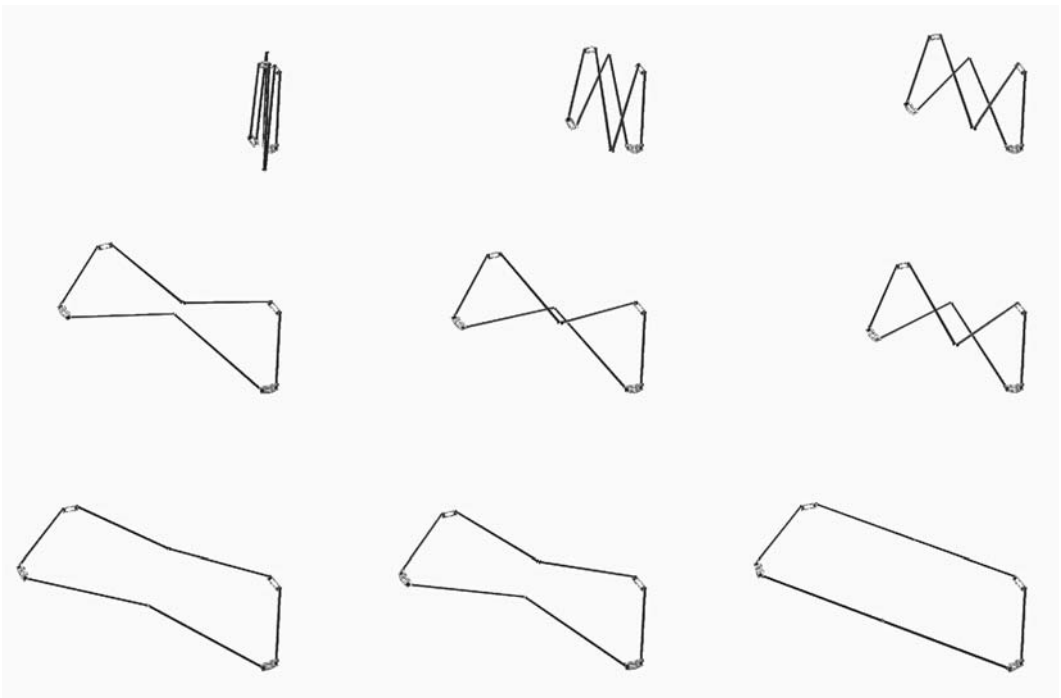

Figure 2.26: Simulation of frame with spur gears in the corners.

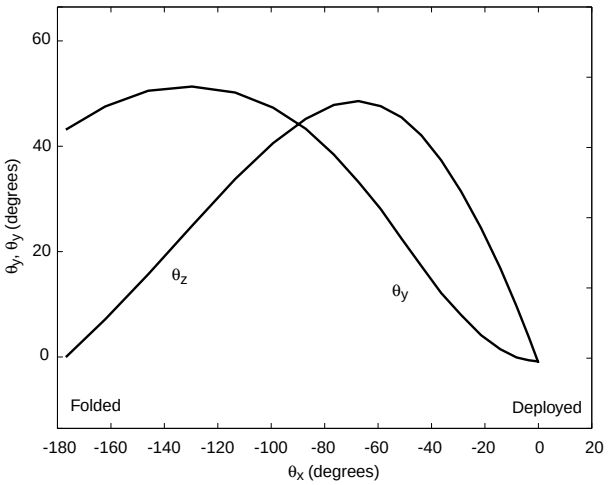

Figure 2.27: Components of rotation of central hinge.

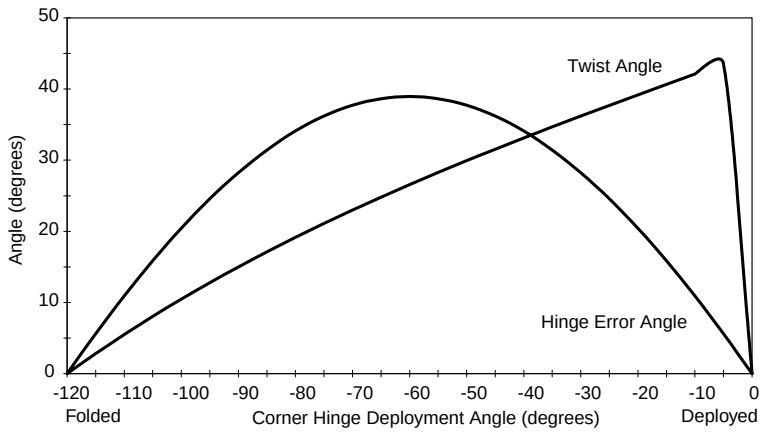

Figure 2.28: Rotations of frame with flexible members, mid-side revolute joints lie in the plane of the frame.

formly, until it reaches a point where the two members become co-axial, at which point the twist angle becomes decoupled from the rotation of the revolute hinges and the two members are allowed to go to the least energy configuration, which is torsionless. This feature can be used to provide an additional locking effect for the frame, which would be in addition to that provided by the tape-spring hinges. Of course, it also means that the strain energy stored while twisting the members may be released in an uncontrolled manner when full deployment is reached.

A way of avoiding this would be to change the direction of the central hinges so that they are naturally at 45° to the plane of the frame. Thus, the structure would start off with elastic strain energy in the twisted members, which would be gradually released during deployment, see Figure 2.29.

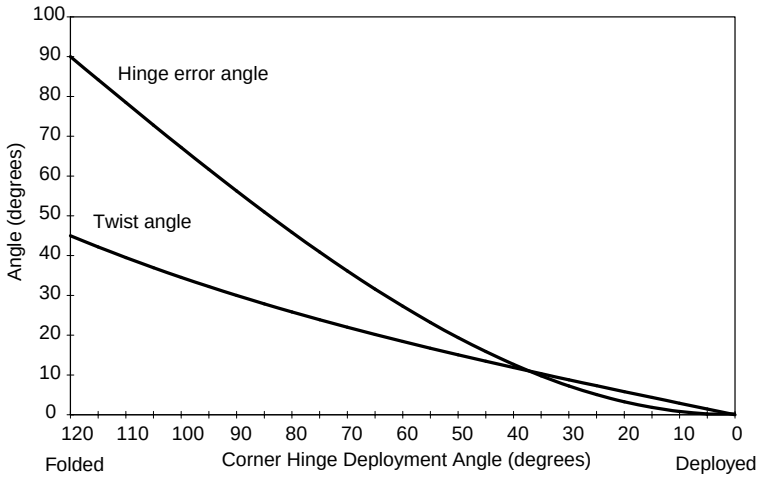

Figure 2.29: Rotations of frame with flexible members, mid-side revolute joints at 45° to the plane of the frame.

Alternatively, the middle hinges could be positioned in a direction somewhere between the two considered above. The structure would then start off with some energy stored in the twisted members, say an initial twist angle of 30°, and then release this energy, with the members twisting 15° beyond their untwisted shape. When the fully deployed configuration is reached, the members would suddenly twist back by 15°, thus locking the mechanism in this configuration. A further development of this idea may lead to frames without self-locking hinges, which are deployed and locked in the deployed configuration purely by the energy stored in the deployed configuration.

A physical model of this concept was constructed with wood end members, Aluminum alloy angle side members, and simple "door" brass hinges, see Figure 2.30. The model confirms that the angle members start with a 45° twist in them and then open out to end in their untwisted shapes, see Figure 2.31.

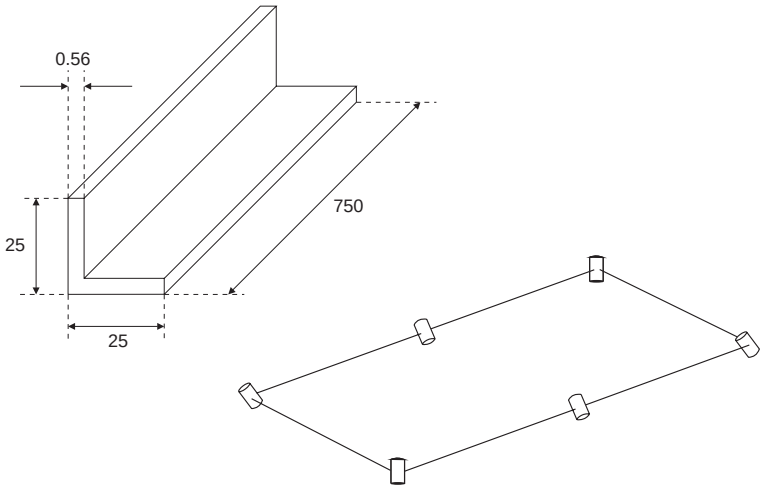

Figure 2.30: Design of frame with flexible members.

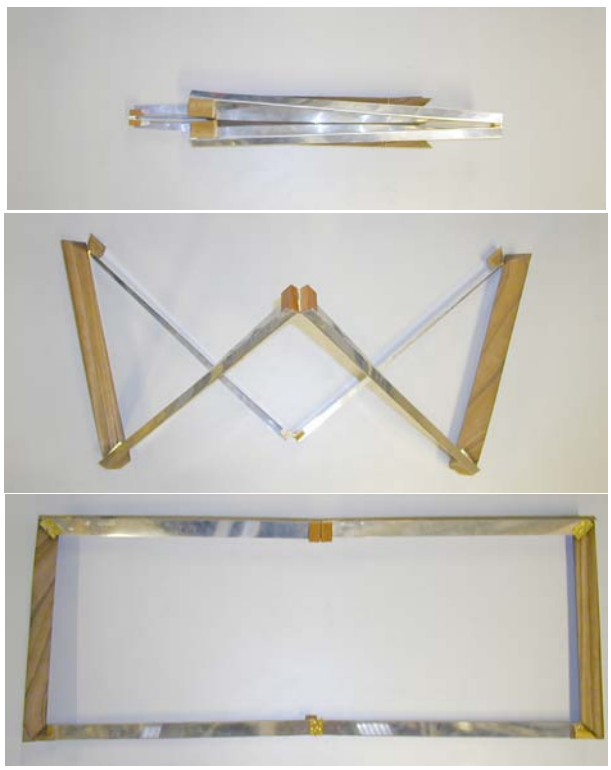

Figure 2.31: Model of frame with flexible members.

2.7 Comparison of SAR dimensions

To illustrate the potential of SAR structures based on the concepts presented in the previous sections, a comparison has been made between the largest SAR structure based on a traditional concept that fits within a specified launcher and the largest structure that could be realised with the new concept. The launch vehicle that was chosen for the comparison is the ROCKOT.

The satellite has to fit within an envelope with radius $r = 1.06$ m, see Figure 2.32 along with a diagram of an existing design for a SAR consisting of three rigid panels, mounted on top of the bus. The two design solutions presented in Section 2.6.5 and 2.6.6 fit into this design envelope with ease.

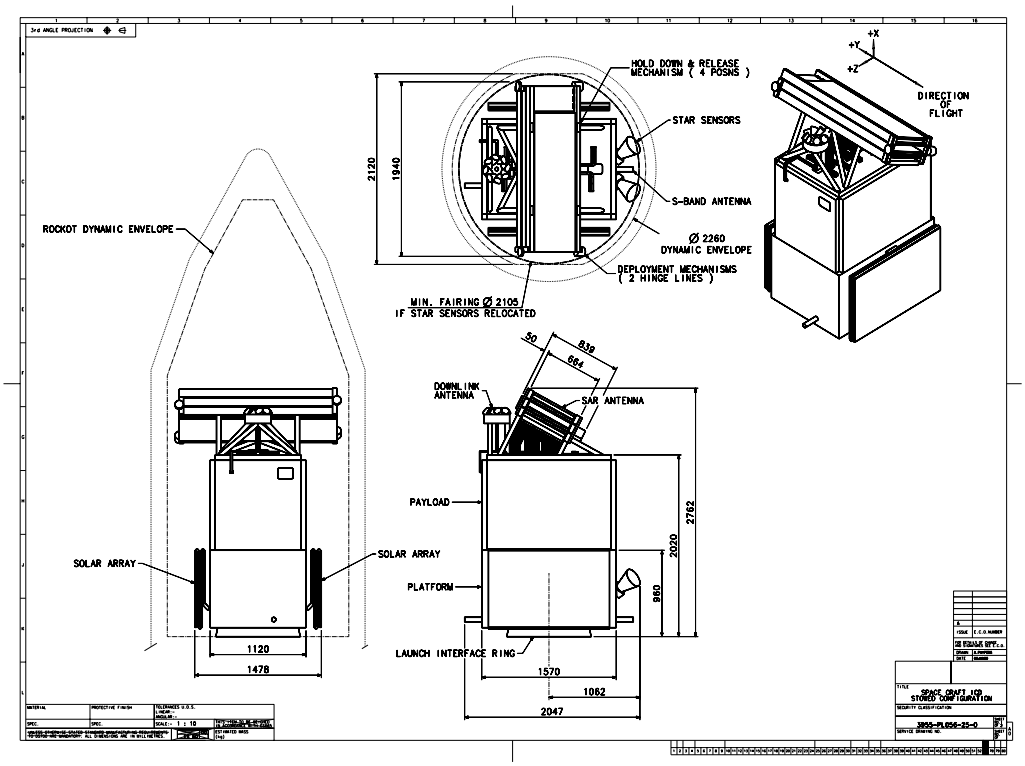

Figure 2.32: Envelope of ROCKOT launcher.

To obtain a preliminary estimate of the maximum SAR size that can fit into the ROCKOT, the configuration shown in Figure 2.33 was considered. The central, rigid panel of the SAR is again mounted on top of the spacecraft bus, inclined at an angle θ. Two foldable frames that deploy and prestress membrane panels are mounted on either side of the rigid panel.

Given the length x of the central panel, the width W and length L (y is the horizontal projection of W) of the rectangular frames are obtained as follows. Note that the thickness of the members of the frame and the separation imposed by the tape spring hinges is neglected in the analysis, for simplicity.

$$W = \frac{\sqrt{(2r)^2 - x^2}}{\cos\theta} \tag{2.3}$$

For $x = 1.2$ m and $\theta = 30°$ Equation 2.3 gives $W = 2.01$ m. This is the limiting value fr both the width of the rectangular frame and its half-length. This gives a maximum array size of $L = 1.2 + 4 \times 2.01 = 9.24$ m by $W = 2.01$ m.

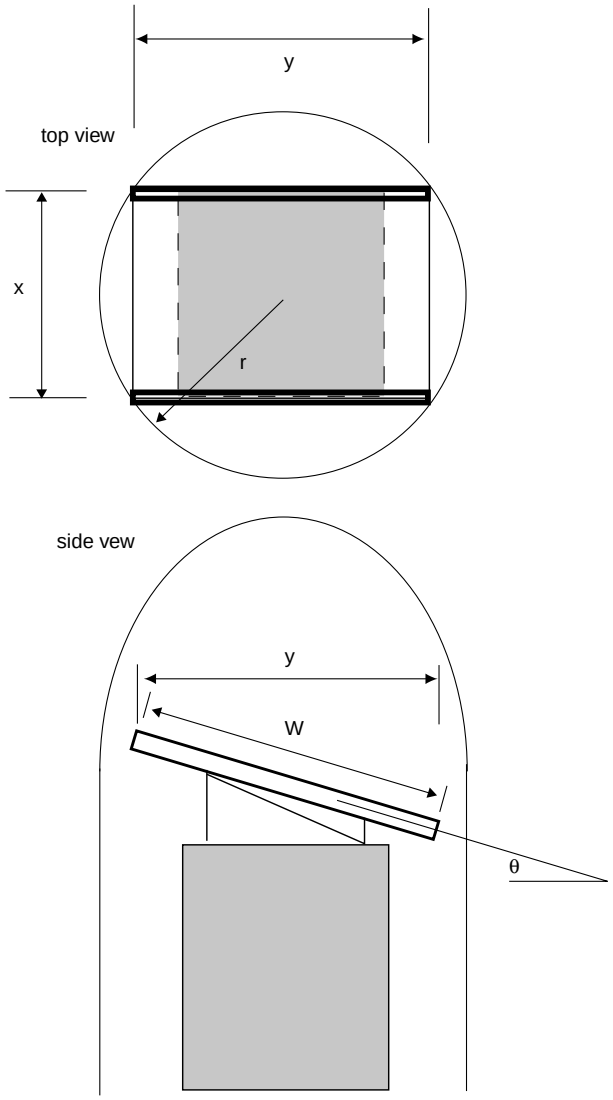

Figure 2.33: Configuration of deployable SAR on ROCKOT vehicle.

A preliminary check that the configuration proposed above does not foul any part of the launcher or the rest of the satellite during deployment has been carried with Pro/Engineer.

2.8 Further Work

More detailed simulations and physical models of the mechanisms described in this report are being developed. Work on determining the configuration of the membrane deployment and pretensioning system is also proceeding.

Once the mechanism choice has been finalised there is much work to do to develop the proposed new concept through to a finalised design. The electrical design of a flexible membrane has to be considered as do the membrane wrapping pattern and detailed design of the mechanism.

2.9 Conclusions

Of the mechanisms that were investigated in this conceptual study, the rigid member frame with 4 revolute and 2 flexible joints, and the frame with flexible members are being investigated further. For the particular application that has been discussed in Section 2.7 these frames can produce SAR structures up to 9 m by 2 m. Compared to the limit of 6 m by 0.7 m for existing technology based on rigid panels, this is a significant improvement.

The use of Pro/Mechanica and the other products within the PTC range has enabled simulations of models to be built. For the simpler configurations that have been examined, these simulations provided the same results as analytical calculations, however with this tool it has been possible to analyse cases that would have been intractable analytically.

The real power of these programs has not yet really been utilised in this conceptual study. The knowledge of the forces within the system as it deploys, including the details of any contact conditions can be used to dynamically model the opening of these frames. based on this, detailed finite element calculations can be made at any stage of deployment. These benefits will become more apparent later in the design cycle when realistic models become harder and more expensive to manufacture and test.

References

Allen, H. G. and Bulson, P. S. (1980). Background to buckling. London, McGraw-Hill.

Auternaud, J., Bartevain, J., Bertheux, P., Blanc, E., de Mollerat du Jeu, T., Foucras, J., Louis, M., Marello, G., Poveda, P. and Roux, C. (1992) Self-motorized antifriction joint and an articulated assembly, such as a satellite solar panel, equipped with such joints. United States Patent no 5,086,541.

Bazant, Z. P. and Cedolin, L. (1991). Stability of Structures. Oxford, Oxford University Press.

Blanc, E. (1990). ADELE Articulation de Deploiement a Lames d'Enroulement. In Proc. Fourth European Symposium on Space Mechanisms and Tribology, Cannes, France, 20-22 September 1989 pp 155-158. ESA SP-299.

Chironis, N. P. and Sclater, N. (1996). Mechanisms and mechanical devices sourcebook. Second Edition. New York, McGraw-Hill.

Curlander, J.C. and McDonough, R.N. (1991). Synthetic Aperture Radar : Systems and Signal Processing. Wiley.

Feria, V.A. Lou, M.C. Huang, J. and Speer (1998), Lightweight Deployable Space Radar Arrays. In 39th AIAA/ASME/ASCE/AHS/ASC Structures, Structural Dynamics and Materials Conference AIAA, 20-23 April 1998, Long Beach, California, pp. 1871-1875.

Laloi, N. (1999). Analytical and experimental study of a new type of hinges. Deployable Structures Laboratory, Department of Engineering, University of Cambridge.

Lou, M. C., Feria, V. A. and Huang, J. (1998), Development of an Inflatable Space Synthetic Aperture Radar. In 39th AIAA/ASME/ASCE/AHS/ASC Structures, Structural Dynamics and Materials Conference AIAA, 20-23 April 1998, Long Beach, California, pp. 2783-2788.

Luhmann, H. J., Etzeler, C. C. and Wagner, R. (1989). Design and verification of mechanisms for a large foldable antenna. In Proc. 23rd Aerospace Mechanisms Symposium, 3-5 May, Marshall Space Flight Center, Huntsville, Alabama pp 113-126. NASA-CP-3032.

Parametric Technology Corporation (1999). Pro/ENGINEER Release 2000i, http://www.ptc.com

Seffen, K. A. and Pellegrino, S. (1997). Deployment of a rigid panel by tape-springs. Department of Engineering, University of Cambridge Report CUED/D-STRUCT/TR168.

Seffen, K. A. and Pellegrino, S. (1999). Deployment dynamics of tape springs. Proceedings of the Royal Society of London, series A 455(1983): 1003-1048.

Szyszkowski, W., Fielden, K. and Johnson, D. W. (1997). Self-locking satellite boom with flexure-mode joints. 50, S225-S231.

Timoshenko, S. P. and Gere, J. H. (1961). Theory of Elastic Stability. New York, McGraw-Hill.